Materials Today • Volume xxx, Number xx • xxxx 2022

ELSEVIER

Emerging application of 3D-printing techniques in lithium batteries: From liquid to solid

Xuejie Gao [1,2,#], Matthew Zheng [2,#], Xiaofei Yang [2], Runcang Sun [1,*], Jiujun Zhang [3,4], Xueliang Sun [2,*]

[1] Center for Lignocellulosic Chemistry and Biomaterials, College of Light Industry and Chemical Engineering, Dalian Polytechnic University, Dalian 116034, China
[2] Department of Mechanical and Materials Engineering, University of Western Ontario, London, Ontario N6A 5B9, Canada
[3] Department of Materials Science and Engineering, Fuzhou University, Fujian 350108, China
[4] Institute for Sustainable Energy/College of Sciences, Shanghai University, Shanghai 200444, China

There is rapid progress in the field of 3D printing technology for the production of electrodes, electrolytes, and packages of batteries due to the technique's low cost, a wide range of geometries printable, and rapid prototyping speed by combining computer-aided design with advanced manufacturing procedures. The most important part of 3D printing applied in batteries is the printing of electrodes, electrolytes, and packages. These will affect the battery energy/power density. However, there are still several challenges that need to be overcome to print active and stable electrodes/electrolytes for energy storage systems that can rival that of the state-of-the-art. In this review, the printing materials, and methods for batteries from liquid to solid-state batteries are discussed and recent examples of this technique applied in high power/energy batteries are highlighted. This review for batteries will cover 3D printing technologies, printed cathode, and anode in conventional batteries, and printed solid-state electrolytes in solid-state batteries. The working principles, advantages, and limitations for solid-state batteries via the 3D printing method will be discussed before highlighting the printing materials for electrodes and electrolytes. We will then discuss how to modify the electrode and solid-state electrolyte to raise the electrochemical performance of solid-state batteries using 3D printing. Finally, we will give our insights into the future perspectives of this printing technique for fabricating batteries.

Keywords: 3D-printing; Conventional Li battery; Solid-state Li battery; High-energy-density battery

Introduction

3D-printing applied in the energy storage system

Energy storage systems are an integral part of electronic devices and the demand for increased energy density batteries is constantly growing [1]. Over the years, great efforts have been made in exploring new electrode materials, electrolytes, battery structures, and novel manufacturing methods to improve the electrochemical performance of batteries, reduce manufacturing cost, and expand their commercial applications [2]. Conventional manufacturing techniques for energy storage systems are complex and expensive processes that are limited in their control of the geometry and architecture of the electrode, ability to develop solid-state electrolytes (SSEs), and cell packaging design. Simultaneously, over the years there has been a growing demand for portable electronic devices with ever-shrinking footprints. This means that a thicker battery electrode must be built to

* Corresponding authors.
E-mail addresses: Sun, R. (rcsun3@dlpu.edu.cn), Sun, X. (xsun9@uwo.ca).
# These authors contributed equally to this manuscript.

 https://doi.org/10.1016/j.mattod.2022.07.016

Please cite this article in press as: X. Gao et al., Materials Today, (2022), https://doi.org/10.1016/j.mattod.2022.07.016

increase the active material loading without reducing ion migration. This will further improve the areal capacity and the energy density of devices [3]. However, it is worth noting that the ion transport distance is increased in thicker 2D electrodes, and therefore interfacial resistance is also raised, which can result in reduced rate capability and energy density. Therefore, it is necessary to design a 3D structure in electrodes due to the shorter ion diffusion pathways and smaller resistance.

3D printing is a newer manufacturing technique for creating a 3D structure through a layer-by-layer deposition process controlled by computer-aided design (CAD) software [4]. The technology is rapidly developing and quickly becoming the basis for the next generation of energy storage systems where batteries could be printed in any shape. One of the strongest advantages of 3D printing is the ability to fabricate complex 3D objects via interpreting CAD models. A further strength is the technique's ability to deposit phase change and reactive materials and solvent-based inks. This fabrication method begins with the design of a 3D virtual model that is sliced into several 2D horizontal cross-sections [5]. By successively printing new 2D layers on top of previous layers, a coherent 3D object can be fabricated. Until now, electronic products have designed their devices according to the size and shape of commercially available batteries, such as cylindrical or rectangular shapes like the coin cell and/or pouch cell, which occupy a significant majority of space in modern electronic devices [6]. Additionally, it is easy to control the thickness of the final printed part by adjusting the number of printed layers. In battery design, this can be leveraged to achieve control of overactive material loading. Batteries further benefit from 3D structured electrodes designed by 3D printing as fast ion migration in thicker electrodes further improve the rate capability of batteries. Overall, 3D printing has several significant advantages as compared with conventional battery fabrication technologies: (1) enable the fabrication of desirable complex architectures; (2) precise control of the shape and thickness of the electrodes; (3) printed solid-state electrolytes can obtain higher structural stability and safer operation; (4) potential for lowered manufacturing cost, increased environmental friendliness, and easier operation; and (5) possibility to eliminate the need for device assembly and packaging via directly printing batteries and other electronics. 3D printing opens new avenues for the rapid fabrication of 3D-structured batteries with complex architectures and high performance.

From liquid to solid-state electrolyte batteries

Solid-state batteries (SSBs) have attracted increasing attention as one of the most promising next-generation batteries [7]. SSBs use a solid-state electrolyte (SSE) to achieve the ionic conduction and electronic insulation traditionally performed by an organic liquid electrolyte and separator. By tuning the composition of the SSE, SSBs can meet the requirement of both safety and performance [3b]. However, various challenges are remaining for SSBs that currently limit practical applications [8]. Particular challenges exist at the interface between the solid-state electrolyte and the electrodes. Interfacial issues are the most important factors affecting resistance in the SSBs [9]. 3D printing can fabricate novel 3D-architectured electrodes with a larger surface area at the interface and enable higher areal-loading density in the battery. Printed electrodes further provide shorter diffusion pathways and smaller resistances during the ion-transport process, which improve battery energy density and power density.

In this manuscript we review the state-of-the-art advances in 3D printing of batteries, focusing on aspects related to the battery component, electrodes, electrolytes, and full batteries from liquid to solid-state batteries. 3D printed separators are not discussed due to their limitations compared to commercial separators. The printing techniques, advantages, and disadvantages of different types of printing methods in terms of printing the cathode, anode, and SSEs are described briefly. Finally, a conclusion and outlook are provided, pointing out avenues for future research.

Fig. 1 maps the timeline of 3D printing and the technique's contribution to battery development from liquid to solid developed in the last several years. Stereolithography (SLA) is a printing technique that was first developed in 1987 by Charles Hull and uses an ultraviolet (UV) laser to induce polymerization to a photopolymer resin [10]. After that point, various 3D printing methods were gradually applied in the field of batteries, such as Fused deposition modeling (FDM), selective laser sintering (SLS), direct ink writing (DIW), inkjet printing (IJP), and other printing techniques. Recently in literature, it was reported that Li-ion micro-batteries can be designed by 3D printing. K. Sun and co-workers developed the SLA 3D-printed micro-battery composed of high-aspect-ratio anode and cathode micro-arrays [10]. Most past works have been focused on conventional lithium batteries, however, in parallel with the pursuit of the high volumetric and gravimetric energy density of lithium batteries, some quasi/full solid-state batteries have been gradually proposed, such as quasi-solid-state Li batteries (QSSLBs) [11], solid-state Li batteries (SSLBs) [12], and solid-state Li-S batteries (SSLSBs) [13].

Considering the compatibility among the preparation conditions, materials, and processes, not all the 3D printing technologies and current materials used in conventional batteries are appropriate for manufacturing printed batteries. A qualitative comparison of different 3D printing techniques for printed batteries is shown in the table below.

Classifications of 3D printing technology applied in the battery

Fused deposition modeling (FDM)

Fused deposition modeling (FDM) printers are the most used printers for fabricating polymer parts [14]. Thermoplastics such as PC, ABS, and PLA, are commonly used as feed material due to their low melting temperature. FDM printers work by controlled extrusion of thermoplastic filaments, as shown in Table 1. In FDM, filaments melt into a semi-liquid state at the nozzle and are extruded layer by layer onto the build platform where layers are fused and then solidify into final parts. The quality of printed parts can be controlled by altering printing parameters, such as layer thickness, printing orientation, raster width, raster angle, and air gap. One common drawback of FDM printing is that the printed materials must be in a filament form to enable the extrusion process. It is difficult to homogeneously disperse reinforcements and remove the void formed during the manufactur-

Please cite this article in press as: X. Gao et al., Materials Today, (2022), https://doi.org/10.1016/j.mattod.2022.07.016

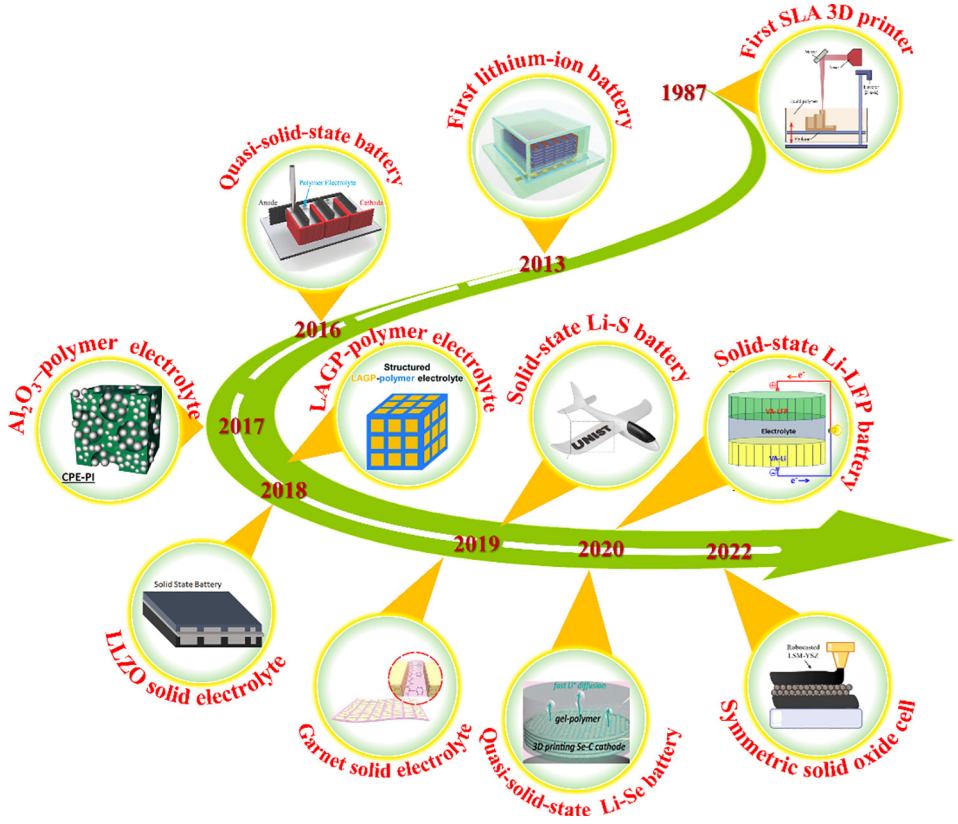

FIGURE 1

A timeline of 3D printing methods applied in batteries from liquid to solid-state batteries.

TABLE 1

Precursor materials, advantages, and disadvantages of popular 3D-printing techniques utilized for battery applications.

3D printer	Working mechanism	Usually printed materials	Advantages	Disadvantages	Application in batteries
SLA	hardened by applying focused light or UV light	curable photopolymer–typically a liquid resin	high accuracy, smooth surface finish	limited pallet of resin materials, printed objects difficult to remove,	package, electrolyte
IJP	propelling droplets of ink onto substrates	Carbon-based, metallic, and polymer materials, even biomaterials can be used	high printing resolution (<50 μm), reduction of material waste, ability to print large areas	limitation of printable inks, low printing speed, limited to thick electrode fabrication, Poor long time durability	electrode
DIW	Materials' ink is deposited in a layerwise method, by the continuous rising of the print head	The flexibility of printable materials, ranging from polymer gels to high shear thinning colloidal	Easy operation, low cost, a wide choice of materials, any shape at room temperature	Harsh requirements on the rheological properties of inks	electrode, electrolyte
FDM	Layer-by-layer through the heated extrusion print head	acrylonitrile–butadienestyrene (ABS), polylactic acid (PLA)	low cost, high speed, large size capabilities, great mechanical properties, printed objects easily removed	low printing resolution, limitation of thermoplastic at elevated temperature (below 200 °C), low electrical conductivity for electrode	package
Others	(SLM) electrode	a high-powered laser to successively melt each layer of the powdered material	any thermally fusible powder material within an operatable temperature range	create metal structure, Low cost, Weight reduction of parts, Shorter time to market	the roughness of the printed material surface

ing of filaments. Another disadvantage of FDM printers is that the printable material is limited to thermoplastic polymers with suitable melt viscosity. Specifically, the molten viscosity should be high enough to provide structural support and low enough to enable extrusion. Another challenge that FDM printers face is the difficulty of completely removing the support structure

Please cite this article in press as: X. Gao et al., Materials Today, (2022), https://doi.org/10.1016/j.mattod.2022.07.016

used during printing. Despite these drawbacks, FDM printers offer several advantages, including low cost, high printing speed, and simplicity [15]. Another advantage of FDM printing is the potential to allow the deposition of diverse materials simultaneously. Multiple extrusion nozzles loaded with different materials can be set up in FDM printers, such that the multi-material printed parts can be endowed with multiple functionalities.

Stereolithography (SLA)

SLA printing uses the process of polymerizing photopolymers by a UV laser. In this process, a UV-laser follows a set path in the resin reservoir, which causes the photocurable resin to polymerize into a 2D patterned layer. After one 2D layer is cured, the platform lowers, and another layer of uncured resin is ready to be patterned [17]. Some polymer materials typically used in SLA printing are acrylic and epoxy resins [18]. Understanding the curing reactions occurring during polymerization is critical to controlling the quality of final printed parts. The intensity of laser power, scan speed, and duration of exposure all affect the curing time and printing resolution. Photoinitiators and UV absorbers can be added to the resin to control the depth of polymerization. The main advantage of SLA printing technology is the ability to print parts with high resolution. Additionally, because SLA is a nozzle-free technique, the problem of nozzle clogging can be directly avoided. However, the high cost of this system is the main concern for industrial applications. Possible cytotoxicity of residual photoinitiators and uncured resin is another concern. This kind of printing method is usually used as a package and solid-state electrolyte for batteries [19].

Direct ink writing (DIW)

DIW technique is based on extruding a viscous material from a pressurized syringe with different needle sizes to create a 3D shape of materials [21]. The syringe head can move in three dimensions, while the platform keeps stationary. Extruded materials are joined together, layer by layer. The curing step usually can be further performed by dispensing two reactive components, using mixing nozzles, or being induced either by heat or UV light in certain cases. The viscosity and deposition speed of the printing materials correlate with the quality of the final printed parts. The key advantage of this technique is the flexibility of material choice(s), which is better for battery applications [22]. Furthermore, DIW can facilitate a wide range of feed materials such as solutions, pastes, and hydrogels. As well, multi-material printing is achievable through a multi-nozzle printer or by utilizing a print–pause–print strategy and swapping syringes (containing different materials). A temporary, sacrificial material may be needed to support the printed structure for DIW printing as the raw printed slurry material generally will have low stiffness that may result in the collapse of complex structures [23].

However, successful DIW printing requires the preparation of ink that can exhibit suitable viscoelastic and shear thinning properties, achievable by tuning the composition of the ink. The printed ink must thus resist gravity-induced deformation (slumping) and capillary forces that attempt to reduce the surface energy of the printed ink by deformation.

Other techniques

Recently, several new techniques have been developed for 3D printing of composites, such as PolyJet which works by polymerization of deposited droplets of photopolymer ink, digital light processing (DLP) which is based on selective polymerization of an entire surface of photopolymer by a projector light [24], liquid deposition modeling (LDM) which consists of the additive deposition of material layers directly from a solution in a volatile solvent [25], and fiber encapsulation additive manufacturing (FEAM) which involves directly encapsulating fiber within an extruded flowable polymer matrix [26]. As compared to traditional 3D printing techniques, these methods have either more material selections or faster processing time. However, due to their high cost and complexity, few research efforts have adopted these new techniques. Powder-based 3D printing techniques, such as Selective Laser Sintering (SLS) or Binder Jetting (BJ) are emerging printing technologies with significant application potential in battery design. These techniques are discussed in Section 5, where we discuss the cutting-edge techniques in printing technologies and future printing trends.

Therefore, the most established types of 3D printers for Li batteries usages are SLA, FDM, and DIW. This review focus on the available 3D printing technologies which is suitable for the battery design, including conventional Li batteries and solid-state Li batteries. As shown in Table 1, summarized the characterization of different types of printing methods. It paves the way for further the application of 3D printing in Li batteries.

Electrode in lithium batteries

Li-battery cathode

Recently, the 3D printing technique has been a promising technology in battery applications [27]. Since different kinds of printing materials can be used in this technique, this allows us to vary the 3D structure of electrodes, electrolytes, separators, and packaging in batteries. The first 3D printing technique applied in LIBs by using DIW was reported by Sun et al. [10]. In this work, the authors designed and optimized both inks of LTO as anode and LFP as cathode for printing. 3D interdigitated microbatteries were directly printed with that approach, yielding optimized electrodes with high aspect ratio electrode architectures. Benefiting from the strong design, the micro batteries exhibited a high areal energy density of 9.7 J cm^{-2} at a power density of 2.7 mW cm^{-2}. Sun et al.'s work found a new insight to demonstrate micro batteries with high energy/power density by using a 3D printing technique. However, parameters affecting printing electrodes were not clear so Kohlmeyer et al. reported the influence printing parameters had on the resulting rheological, electrochemical, and mechanical properties [28]. In that work, 3D-printable and free-standing electrodes of three common LIB active materials, $Li_4Ti_5O_{12}$, $LiFePO_4$, and $LiCoO_2$ were prepared by using the DIW method, which utilized a well-dispersed mixture of active materials, CNFs, and polymers to make printable electrode slurry. The author found that every component can play a significant role to improve the overall performance of the printed electrode, for example, the addition of CNFs can promote conductivity; the addition of polymers improves the viscosity and mechanical properties of the electrode, and adding active materials varied the cell's electric storage capacity. Therefore, each printed elec-

Please cite this article in press as: X. Gao et al., Materials Today, (2022), https://doi.org/10.1016/j.mattod.2022.07.016

trode delivered good cycle ability and rate capability. Considering the advantage of the 3D printing method for batteries, many variations of cathodes can be printed and then applied to batteries. For example, a 3D-printed LIB based on LMFP nanocrystals was developed by Dr. Pan's group, as shown in Fig. 2(a) [29]. In this work, the 3D structure of the printed slurry LMFP was built with printing height and width of 18 and 450 μm, respectively. When the battery was assembled with 3D-printed LMFP, it demonstrated a capacity of 108.45 mAh g^{-1} at 100C and a reversible capacity of 150.21 mAh g^{-1} at 10C after 100 cycles. Compared with the traditional electrode, this LIB with a 3D-printed LMFP cathode demonstrated ultra-high-rate capacity and capability. The authors also calculated the impact factor of electrolyte diffusion (D_3) on battery rate performance. Further details were measured such as solution intrinsic diffusion coefficient (D_{3A}), efficiency porosity (D_{3B}), and electrode thickness (D_{3C}), which all can play an important role in determining the whole kinetics process in LIBs. Kohlmeyer et al.'s work paved the way to achieve high rate and high-capacity performance for LMFP cathode by using the 3D printing method.

There are many factors to consider when preparing ink-based printing for battery applications. Room temperature printing processes usually can be used to prepare 3D electrodes. One important factor during the printing process is to maintain the structural integrity and strength of printed features. However, the electrode ink for printing must easily flow and must maintain the printed 3D shape for a long time. Hence, a low-temperature direct writing (LTDW)-based 3D printing was for the first time used to prepare LFP electrodes in batteries by Liu et al. As shown in Fig. 2(b), a porous structure was demonstrated in the printed LFP electrode. During the printing process, the low temperature was used to freeze the electrode and maintain its printed shape such that the biomaterial scaffolds with interconnected pores could be fabricated. Benefiting from that, the LFP electrode with improved porosity facilitated electrolyte infiltration and Li-ion transport, therefore enhancing the rate performance of LIBs. By precisely controlling electrode geometry and structure, 3D-printed electrodes can improve ion/electron transport. Moreover, the thickness and active material loading can be directly controlled by adjusting the number of printed electrode layers. 3D printing can also have a big role in Li-batteries. Shen et al. for the first reported a 3D sulfur copolymer–graphene architecture (3DP-*PSG*) with a well-designed grid structure for Li-S batteries through the 3D printing approach [30]. This printed cathode was fabricated based on an ink composed of sulfur particles, 1,3-diisopropenylbenzene (DIB), and condensed graphene oxide. The aforementioned study demonstrated the advantages of 3D printing applied in the fabrication of thick sulfur cathodes. The work produced cathodes with a thickness of 600 μm by stacking 6 printed layers. When the Li-S battery was assembled with a 3DP-*p*SG cathode, it delivered a reversible capacity of 812.8 mAh g^{-1} and capacity retention of just 43.4% within 50 cycles at 50 mA g^{-1}. These performances of the results were mainly attributed to the low electronic conductivity of the sulfur copolymer and the poor Li^+/e^- transport in the printed thick electrodes. Therefore, it is still necessary to find ways to optimize the 3D printing process to further ensure high electrochemical performance in Li-S batteries [3c,d]. Our group recently has shown a 3D-printed lithium-sulfur cathode to fabricate a thick electrode with a porous structure at macro, micro, and nanoscale [31]. As shown in Fig. 2(c), the 3D-printed high sulfur-loading cathode was employed in Li-S batteries. In this work, the ink for 3D printing is composed of the sulfur/carbon (S/C) active material, acetylene black (AB), commercial carbon nanotubes (CNTs), and polyvinylidene fluoride-hexafluoro propylene (PVDF-HFP) as the binder dissolved in 1-methyl-2-pyrrolidinone (NMP). The porosity of the electrode structure was further optimized by 3D printing combined with phase inversion to produce pores at the macroscale and the nanoscale. This feature helped enable facile electronic and ionic transportation in the thick cathode, which improved the electrochemical performance of the final 3D printed cathode with a hierarchical porous structure. Therefore, when Li-S batteries were assembled with the printed cathode at a sulfur loading of 5.5 mg cm^{-2}, the battery delivered a large initial specific discharge capacity of 912 mAh g^{-1} at a rate as high as 2C, equaling to high areal current densities of 18.4 mA cm^{-2}. Our previous work offered a new strategy to fabricate high sulfur loading cathodes and improve the electrochemical performance including cycling stability and rate performance for Li-S batteries [32]. However, even with this optimization from macroscale to nanoscale by 3D printing combined with the phase inversion method for Li-S cathode, performance still suffered from capacity decay with increased sulfur loading due to the prolonged and tortuous Li^+/e^- transport in the thick electrode [32]. We further improved our technique by developing a thickness-independent electrode with high sulfur loading Li-S cathode by shortening Li^+/e^- migration distance [33]. In this work, 3D disordered thick electrodes were converted into numerous vertically-aligned 2D "thin electrodes" by integrating the 3D printing with an ice-template method. Each of those thin electrodes had a constant thickness of around 20 μm which substantially enhanced local accessibility to Li^+/e^-, enabling similar electrochemical kinetics despite the total thickness of the whole electrode. As a result, highly similar cycling performance and rate performance for Li-S batteries were demonstrated with the 250 μm and 750 μm (i.e., sulfur loadings of 2 and 6 mg cm^{-2}) electrodes. Both two different sulfur loading cathodes delivered a similar capacity of 530 mAh g^{-1} at a current density of 10 mA cm^{-2} and a low-capacity decay of 0.1% per cycle over 200-cycles at a current density of 1 mA cm^{-2}. Another example was reported by Dr. Zhongfan Liu [3c], as shown in Fig. 2(d), a rational design of elaborate V_8C_7–VO_2 heterostructure scaffolds via the 3D printing (3DP) technique was employed as a dual-effective polysulfide immobilizer and lithium dendrite inhibitor for Li–S batteries. Therefore, this electrode demonstrated excellent rate capability (643.5 mAh g^{-1} at 6.0 C) and favorable cycling stability (a capacity decay of 0.061% per cycle at 4.0 C after 900 cycles). This work marks the first-time investigation in solving the obstacles for both S cathode and Li anode throughout the 3D-printing technique and offers a clear path forward for the development of high safety, long lifespan, and advanced energy Li–S batteries.

Benefiting from the 3D printing technology has been an effective way to achieve high energy and power density by increasing the mass loading of active materials. Hence, 3D printing has also found more applications in other energy storage devices like Li-

Please cite this article in press as: X. Gao et al., Materials Today, (2022), https://doi.org/10.1016/j.mattod.2022.07.016

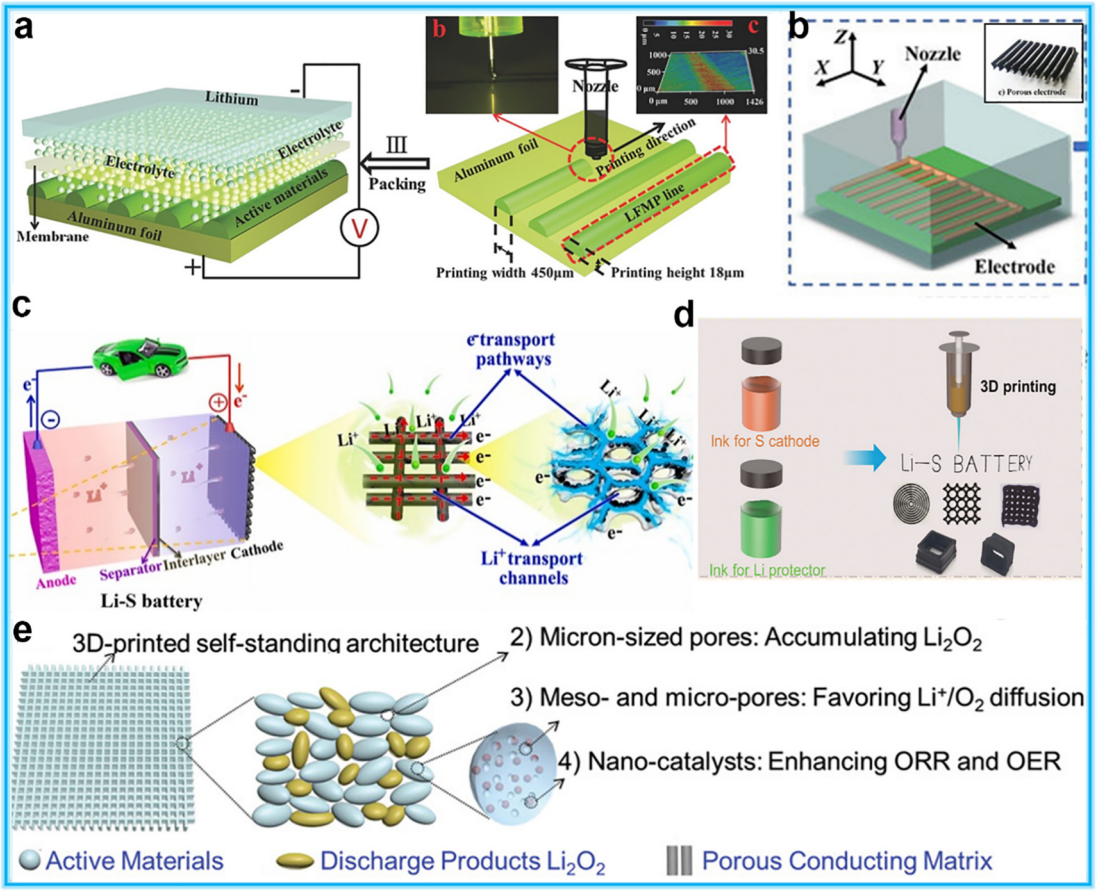

FIGURE 2

(a) Schematic of battery preparation with the 3D-printed electrode with printing width and height of 450 and 18 μm, respectively. (b) Fabrication process of LFP electrode by low-temperature direct writing (LTDW) method with inset optical image of the printing LFP electrode. (c) Schematic illustration of 3DP-FDE applied in Li-S batteries with excellent Li^+/e^- transport in both micro and nanoscale. (d) 3DP process and real photos of 3DP architectures from the prepared homogeneous inks. (e) The novel cathode was designed with a 3D-printed self-standing and hierarchically porous catalyst framework without employing the porous matrix.

CO_2 batteries, Li-O_2 batteries. For example, an effective strategy of combining 3D printing with thermal shock treatment for the fabrication of a thick electrode in a high energy density Li-CO_2 battery was reported by Dr. Hu's group [34]. In this work, a high areal capacity of 14.6 mAh cm^{-2} was achieved due to the thick electrode design and uniform distribution of ultrafine catalyst nanoparticles. In addition, Dr. Hu's group was the first to propose and demonstrate Li-O_2 cathode fabrication by 3D printing [35]. In that work, an additive-free that meshes macroscale and microscale porosity was able to elevate active site utilization as well as mass/ionic transport to improve overall Li-O_2 battery performance. However, in the high-energy–density Li-O_2 batteries, the electrode still suffered from the passivation of cathode surfaces by the insulating Li_2O_2 product. Later research demonstrated 3D-printed self-standing MOF-derived hierarchically porous frameworks for high-energy–density Li-O_2 batteries, as reported by Zhiyang et al. [36]. As shown in Fig. 2(e), the porous framework consisted of micrometer-sized pores formed between Co-MOF derived carbon flakes and micropores formed within the flakes, which (1) possessed good conductivity and mechanical stability, (2) favored the efficient deposition of Li_2O_2, and (3) facilitated the decomposition of insulation Li_2O_2. Therefore, the cell energy was found to be significantly improved by employing this porous cathode with a catalyst architecture. Zhiyang's work showed a new pathway to design a porous network cathode from nanometers to micrometers for realizing the high energy density of the Li-O_2 batteries by 3D printing. In addition, the 3D printing method can also be applied to Na-based batteries due to the controllable thickness, mass loading, and pore size [37].

Li-battery anode

3D printing technology not only has demonstrated use in cathode fabrication but also has great potential for fabrication of the anode part of batteries due to the technique's great control over the electrode's thickness and shape. A high mass loading porous, thick $Li_4Ti_5O_{12}$ (LTO) anode with a thickness of around 200 μm, 450 μm, and 820 μm were printed under low temperature, as reported by Changyong et al, with corresponding mass loading of around 13.3 mg cm^{-2}, 24.1 mg cm^{-2}, and 32.3 mg cm^{-2} [38]. The work demonstrated the difference between material-specific capacities and areal capacities with electrode thickness for the conventional flat electrode and 3D-printed electrodes. As shown in Fig. 3(a), the 3D-printed elec-

Please cite this article in press as: X. Gao et al., Materials Today, (2022), https://doi.org/10.1016/j.mattod.2022.07.016

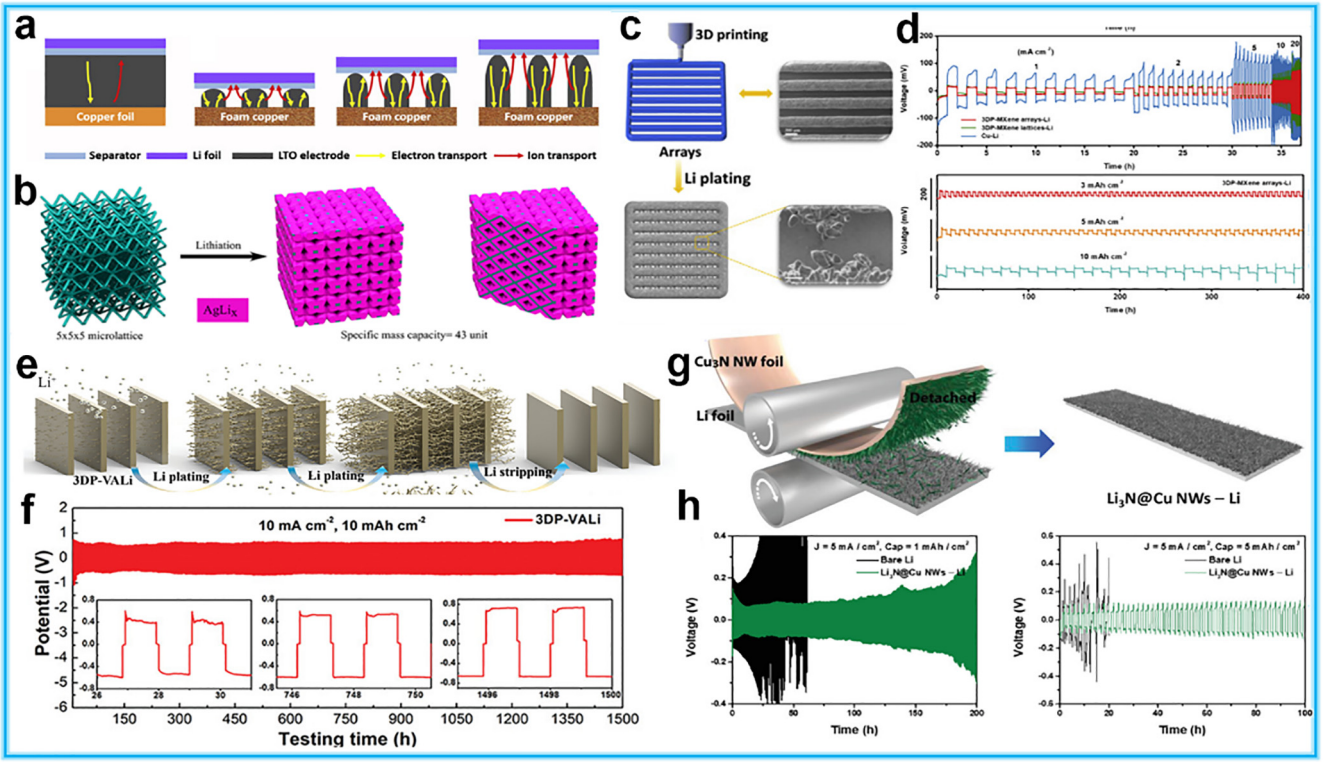

FIGURE 3

3D printing was applied in the anode for lithium batteries. (a) Schematic of electron and ion transport in conventional flat thick electrodes and 3D-printed electrodes. (b) Schematic of the lithiation process for the 3D-printed Ag anode. (c) Schematic of 3D printing MXene arrays and lattices to guide the nucleation and growth of lithium. (d) Rate capabilities of symmetric cells with 3DP-MXene arrays Li, 3DP-MXene lattices-Li and Cu-Li from 1 to 20 mA cm^{-2} and cycling performance 3DP-MXene arrays-Li under various plating-stripping capacities with a constant current density of 1 mA cm^{-2}. (e and f) schematic image of 3DP-Li plating and stripping process, Li–Li symmetric cell performance at a current density/areal capacity of 10 mA cm^{-2}/10 mA h cm^{-2}. (g) Schematic illustration of Cu_3N NWs printing onto bare Li foil by a facile roll-press method. (h) Li-Li symmetric cell test at current densities/areal capacities of 5 mA cm^{-2}/1mA h cm^{-2}, and 5 mA cm^{-2}/5mA h cm^{-2}.

trodes with well-designed architectures were able to achieve high specific capacities and large areal capacities, which can be attributed to the transport distance of Li ions within the electrodes being more constant than that of conventional flat electrodes regardless of electrode thickness. However, such a large thickness of the LTO anode has major challenges, namely, the degradation of the rate capacities at a high rate of 5C due to the slow kinetics in the electrodes. Therefore, the electrode shape design, especially in 3D-printed electrodes, still faces a wide range of significant challenges. There is a work proposed by Mohammad Sadeq et al. to fabricate a complex 3D lattice battery electrode with hierarchical porosity for Li-ion batteries [39]. The 3D electrode demonstrated a strain tolerance to deformation and retention of the shape during the lithiation and delithiation process, as shown in Fig. 3(b). However, both works have demonstrated a low specific capacity and discharge voltage which cannot meet the requirement of electric vehicles.

The lithium metal battery has the potential to be the next-generation energy storage system due to its high theoretical capacity (3860 mAh g^{-1}) and lowest electrochemical potential (−3.04 V vs the standard hydrogen electrode) [40]. This makes lithium metal batteries highly desirable for use in electric vehicles. However, the nonuniform Li deposition during the plating and stripping process has inhibited the lithium metal battery's practical application. A dendrite-free lithium anode was proposed based on 3D printed MXene arrays by Dr. Yang's group [41]. In his work, cobblestone-like lithium was grown towards the direction of the interspaces between two printed filaments within the printed array electrode, which achieved high areal capacities (10–20 mAh cm^{-2}) and low overpotentials of around 10 mV at a current density of 1 mA cm^{-2}. Moreover, the voltage profiles were still stable over 400 h, elevating the areal capacity to a high value of 10 mAh cm^{-2} at a limiting current density of 1 mA cm^{-2} (Fig. 3(c) and Fig. 3(d)). Such good results are mainly attributed to the 3D-printed MXene arrays-Li which provided more electroactive surface area and increased electrochemical reaction rates and facilitated Li^+/e^- transfer during the plating/stripping process. But for the practical application in lithium metal batteries, these results can still not satisfy the requirement of high energy/power density rechargeable batteries, especially at such a low current density of 1 mA cm^{-2}. Therefore, a 3D-printed, vertically aligned Li anode (3DP-VALi) was proposed by our group to achieve that goal [42]. In that work, the Li anode was specifically designed with microscale features for selective "side deposition", where Li preferred to deposit on the micro walls of 3DP-VALi (Fig. 3e). As a result, the Li-Li symmetric cell presented an excellent long cycling life of 1500 h and 400 h at ultrahigh current densities/areal capacities of 10 mA cm^{-2}/10 mAh cm^{-2} and 5 mA cm^{-2}/20 mAh cm^{-2}, respectively, as shown in Fig. 3(f). This result demonstrates a way to realize a goal of a

Please cite this article in press as: X. Gao et al., Materials Today, (2022), https://doi.org/10.1016/j.mattod.2022.07.016

high energy/power density lithium metal battery. Another interesting work to achieve a dendrite-free Li metal featured the introduction of an interlayer between the Li anode and separator. Copper nitride nanowires (Cu3N NWs) printed Li by a facile and roll-press method was reported by Dongsoo et al. [43]. In the aforementioned work, the Cu_3N NWs were printed onto the Li metal surface by a one-step roll pressing method, as shown in Fig. 3(g). The transferred Cu_3N NWs can form a Li_3N@Cu interlayer which has high Li-ion conductivity. Due to the suppression of Li dendrite formation, the Li-Li symmetric cell thereby demonstrated a very stable cycling performance at 5 mA cm^{-2} with a capacity of 5 mAh cm^{-2} over 100hrs. Furthermore, the full cell assembled with Li3N@Cu NWs-Li and LTO showed ultra-long cycling performance at a high rate of 4C over 1000 cycles (Fig. 3(h)). Therefore, introducing an interlayer on Li metal is also a significant way to realize dendrite-free morphologies for lithium metal batteries.

Full batteries

Micro-battery

Recently, 3D micro-batteries have been proven to be highly suitable for the application of micro-electrochemical systems, biomedical sensors, and wireless sensors due to their high energy/power density [44]. Currently, lithium titanate (LTO) and lithium iron phosphate (LFP) is the most commonly used anode and cathode materials in 3D-printed micro-batteries, exhibiting minimal volumetric expansion, high-rate capability, high stability, and security. In a work by Sun et al., a 3D micro battery composed of high-aspect-ratio LTO-LFP electrodes with interdigital architectures was fabricated [10]. Fig. 4(a) shows the interlaced stack of LTO and LFP electrodes that were 3D-printed layer by layer to create the working anode and cathode of a micro battery. When an 8-layer 3D interdigitated micro battery architecture (3D-IMA) was tested as a function of C rate, it delivered around 1.5 mAh cm^{-2} at a working voltage of 1.8 V at a rate of 5C. More importantly, it exhibited a good cycle life of over 30 cycles with a minimum decay in the capacity as shown in Fig. 4(b). This micro battery design could find a potential application in autonomously powered microelectronics and biomedical devices. Benefiting from the liquid electrolyte, this DIW design of micro-batteries can run at a high rate. However, for the FDM/FFF method, polymers are usually a necessary component for micro-batteries [45]. One major hurdle to realizing the goal of the micro battery is the low ionic conductivity of the polymers used for 3D printing. Recently, one article reported 3D-printed complete lithium-ion batteries which employed poly (lactic acid) (PLA) with a mixture of ethyl methyl carbonate, propylene carbonate, and $LiClO_4$ to achieve an ionic conductivity of 0.085 mS cm^{-1} in the electrolyte [46]. Meanwhile, a high capacity can be realized through the contribution of lithium titanate and graphene in the anode, and lithium manganese oxide and carbon nanotubes in the cathode. The authors also demonstrated a 3D-printed coin cell, as well as 3D-printed wearable electronic devices with integrated batteries (Fig. 4c). The aforementioned work created new polymer composites to enable 3D printing of lithium-ion battery anode and cathode. However, high areal loadings electrodes were not fabricated in the work. Therefore, 3D architecture microelectrodes with high loading materials were proposed via DIW technique to realize high areal capacity for lithium-ion micro-batteries, as reported by Zhou et al. [47]. Benefiting from the design of LFP microelectrodes with hierarchical porous structure and the help of 3D printing combined with the freeze-drying method, the electrolyte was able to penetrate the thick electrode and also facilitate Li-ion transport. As a result, the LFO microelectrodes with 32 mg cm^{-2} loading achieved an ultrahigh areal capacity of 5.05 mAh cm^{-2} after 100 cycles. Moreover, when the micro battery was assembled with 3D-printed LFP and LTO as electrodes, it delivered a good electrochemical performance. A full cell assembled with the printed electrodes was used to light a series of light-emitting diodes (LED) with the pattern of CSU, showing the viability of 3D-printed micro-batteries, as illustrated in Fig. 4(d). However, in the reported work, the full cell ran just 35 cycles with a low coulombic efficiency of 82.7%, which cannot meet the real-application requirement of electric vehicles.

A recently reported work focused on high energy/power density micro batteries with 3D printed thick, biphasic semisolid electrodes, as shown in Fig. 4(e) [48a]. That work demonstrated a high areal capacity of 4.45 mAh cm^{-2} at 0.14 mA cm^{-2} (which is equivalent to 17.3 Ah L^{-1}), and also reported full cells delivering a high energy density of 20 mWh cm^{-2} at around 1 mW cm^{-2}. Although there are many developments in micro-batteries by the printing technique, 3D-printed lithium metal batteries have not been reported due to the difficulties of printing lithium metal. In particular, lithium metal has very poor wettability with many substrates and is also highly reactive and reacts easily. For those reasons, there are significant technical challenges with printing lithium metal and a printing technique is yet to be identified. It is worth noting that lithium metal batteries have been regarded as the holy grail of next-generation energy storage systems due to the high energy density of lithium metal and low standard reduction potential (−3.04 V vs standard hydrogen electrode) [48a]. Recent work reported high-performance lithium metal batteries by using 3D printing. The cellulose nanofibers (CNFs) were employed in this work due to the unique shear thinning properties of CNF gel, enabling the printing of an LFP electrode and acting as a stable scaffold for lithium metal. The authors found that the dendrite formation was suppressed by the design of the c-CNF/Li anode. As shown in Fig. 4(f), the symmetric cell of c-CNF/Li delivered outstanding stability with a lower overpotential over 300 h compared with that of bare Li metal symmetric cell, when tested at a current density of 5 mA cm^{-2}. Moreover, the full battery shown in Fig. 4g has a stable specific capacity of 80 mAh g^{-1} over 3000 cycles at a high rate of 10 C. While Dr. Li, et al. reported 3D-printed LFP/LTO electrodes with satisfactory electrochemical performance and mechanical durability under large and repeated stretches and demonstrated the promising potential of such printed electrodes to enable portable, wearable, stretchable and flexible Li-ion batteries [48b].

3D-printing applied in solid-state batteries

Conventional lithium-ion batteries with liquid electrolytes suffer from safety issues and insufficient lifetime [49]. All-solid-state lithium batteries (ASSLBs) have received great attention as the

Please cite this article in press as: X. Gao et al., Materials Today, (2022), https://doi.org/10.1016/j.mattod.2022.07.016

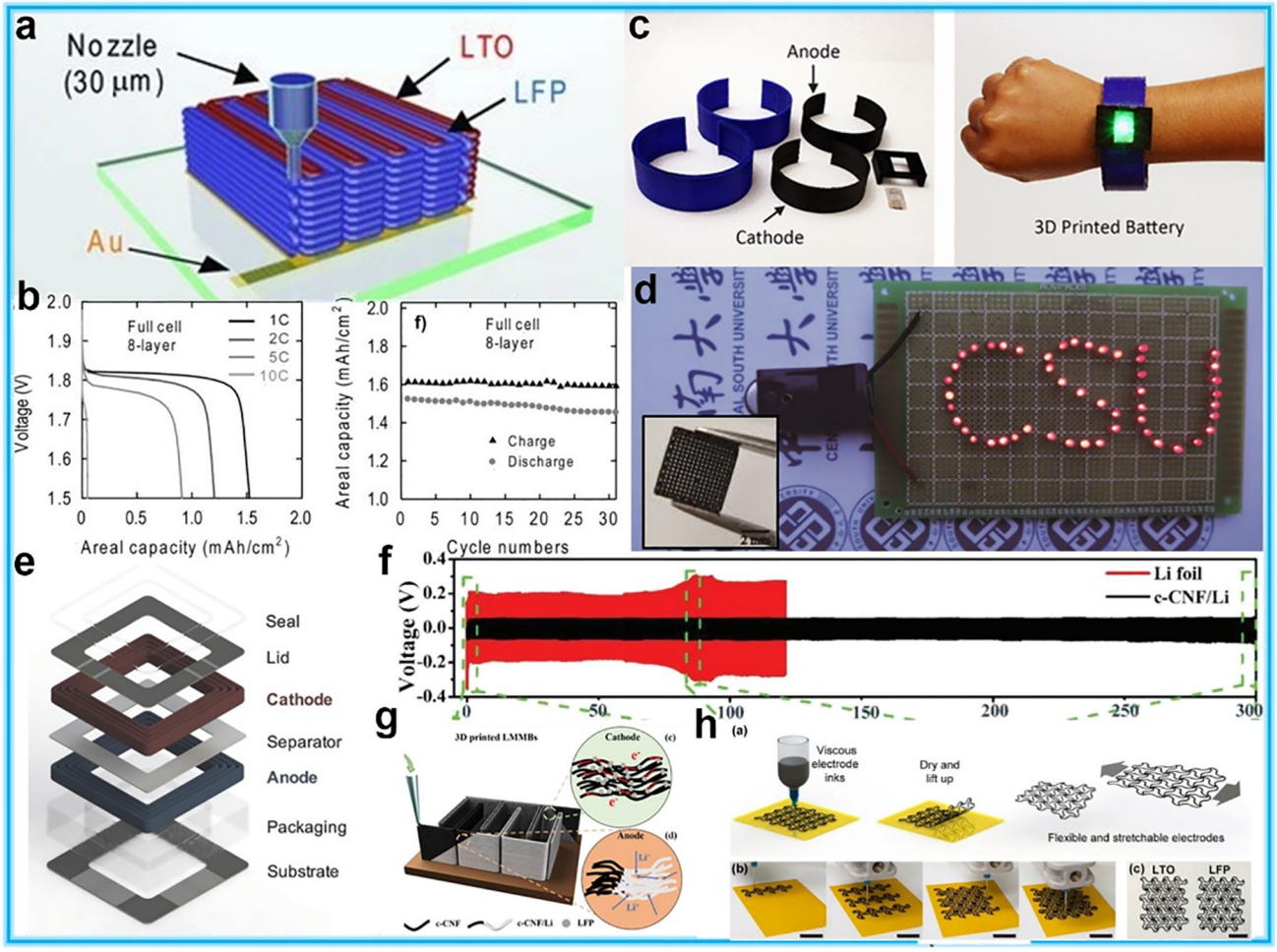

FIGURE 4

(a) Schematic illustration of 3D-printed interdigitated LTO-LFP micro battery architectures. (b) Full cell voltage and areal capacity for 8-layer interdigitated LTO-LFP electrodes. (c) 3D printed components of 3D printed bangle battery with an integrated LED and assembled this battery powering an LED. (d) A lighted LED string with the pattern of CSU (Central South University). (e) Schematic representation of fully 3D printed lithium-ion square cell. (f) Comparison of cycling performance in a symmetric cell at a current density of 5 mA cm^{-2} with an areal capacity of 2.5 mAh cm^{-2}. (g) 3D-printed lithium metal batteries with a high aspect ratio. (h) Suitably patterned stretchable electrodes fabricated by 3D printing.

next step beyond state-of-the-art Li-ion batteries due to their improved safety and energy density [7,27a]. The solid-state electrolyte (SSE) in ASSLBs has the main role in ion transport, and storage, and acts as a separator. Thereby, the SSE has a great influence on electrochemical performance such as cycle and rate capability [50]. There are different kinds of SSEs, such as sulfide-based [7,51], oxide-based [52], polymer [53], and halide electrolytes [54]. With the continuing advances of 3D printing technologies, SSEs can also be directly printed to reduce the fabrication procedures, fabrication time, and manufacturing cost. However, due to the limitation of air stability, sulfide-based and halide-based electrolytes are not suitable to be printed. Therefore, polymer and oxide-based electrolytes are the class of promising SSEs for 3D printing using in ASSLBs.

3D-printed quasi-solid-state batteries

Li-ion batteries

Due to the high ionic conductivity, low cost, environmental friendliness, and safety of polymer electrolytes, polymer SSEs have been attracting significant attention in the energy 3D printing field [55]. Moreover, graphene oxide (GO) has also shown promising printing additives because of its high viscosity and shear-thing behavior, which is well suited to 3D printing [56]. Recently, GO-based electrode composites inks and gel-polymer electrolyte inks were reported to realize 3D-printed solid-state lithium batteries by Dr. Hu's group [11]. As shown in Fig. 5(a), the 3D-printed solid-state lithium battery was composed of lithium-ion phosphate (LFP) as the cathode and lithium titanium oxide (LTO) as the anode. Both electrodes featured highly concentrated GO sheets to bind the electrode materials, and poly (vinylidene fluoride)-*co*-hexafluoropropylene (PVDF-*co*-HFP) with Al_2O_3 nanoparticles as gel-polymer electrolytes. Fig. 5(b) shows the 3D-printed full cell. Both cathode and anode loading is ~18 mg cm^{-2} when normalized to the overall area of the battery. However, during the cell assembly, the liquid electrolyte was injected into the channel between two electrodes to fully soak the electrodes and serve as the polymer electrolyte. However, this design of a 3D-printed battery should be more specifi-

Please cite this article in press as: X. Gao et al., Materials Today, (2022), https://doi.org/10.1016/j.mattod.2022.07.016

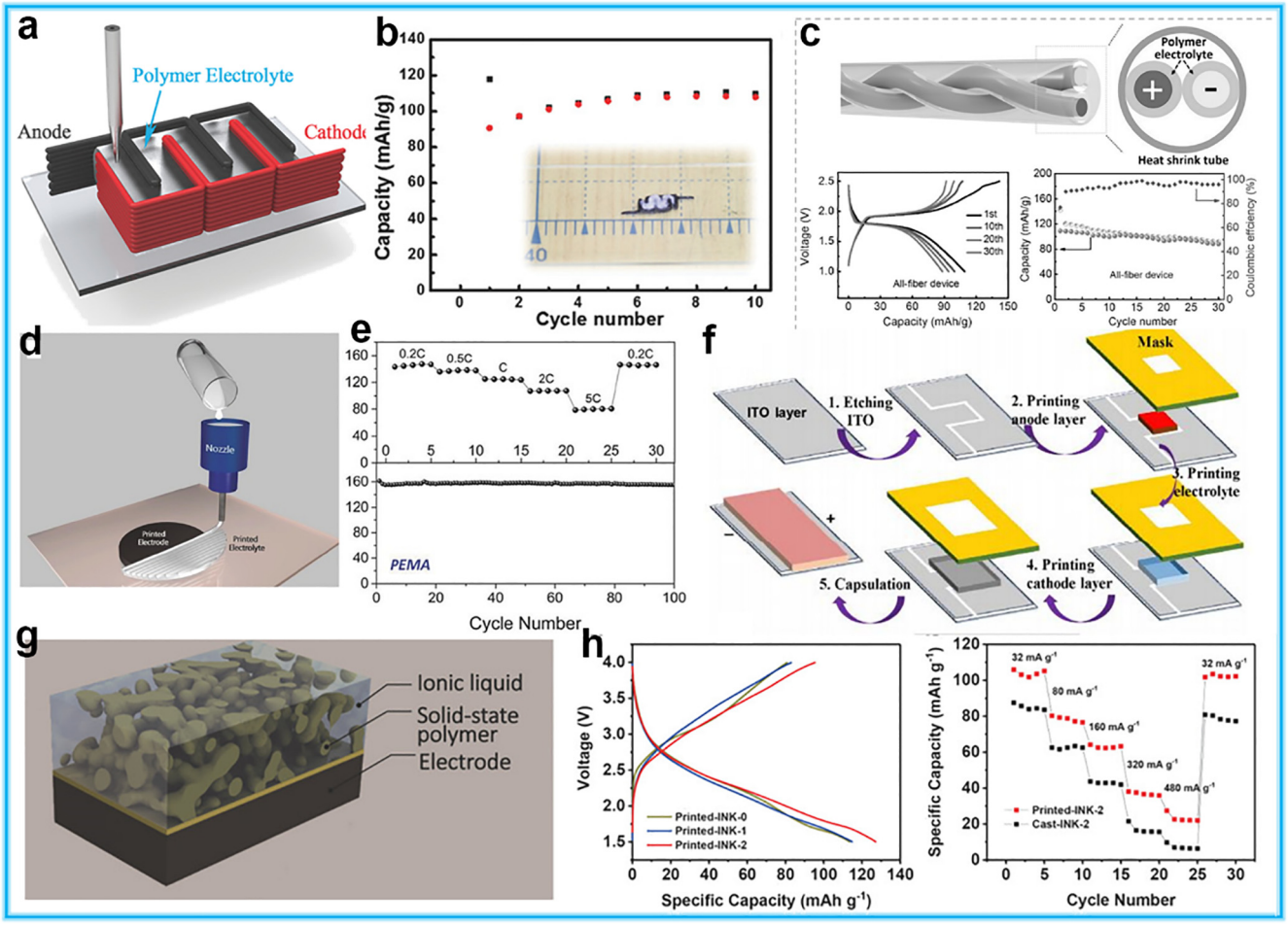

FIGURE 5

(a) Schematic of the 3D-printed interdigitated electrodes and electrolytes for the solid-state battery. (b) Cycling stability of the 3D-printed full cell. The inset is a digital image of the 3D-printed full cell consisting of LFP-rGO, LTO/ago, and polymer electrolyte. (d) Schematic illustration of the filamentary printing process. (e) Rate performance (top) and cycling performance (0.2C, bottom) of the PEMA configuration. (f) Schematic of the assembly procedure for a full solid-state lithium-ion battery (FSLB) with the designed architecture. (g) Schematic of the printed hybrid solid-state electrolyte. (h) First cycle-discharge voltage profiles of MnO_2/Li with printed electrolyte at a specific current of 16 mA g^{-1} (left), and rate profiles of Li/MnO_2 half-cell with printed/cast INK-2 electrolyte at various specific currents.

cally delineated as a quasi-solid-state lithium battery (QSSLB) rather than an ASSLB [57]. A low-cost micro battery was fabricated by employing an ink-jet printed ion gel electrolyte and porous composite electrode [58]. In that work, the LFP cathode and LTO anode porous electrodes were both coated by an ion gel solid electrolyte layer and were inserted face to face in a Swagelok cell to fabricate a lithium-ion battery. It should be noted that a fiberglass separator soaked in PYR14-TFSI and Li-TFSI solution was nevertheless inserted to promote a good wetting contact between the two-solid electrolyte ion gel surfaces, thereby categorizing that work as a QSSLB. Another example of 3D-printed QSSLB was also proposed by Dr. Hu's group [59]. In Hu's work, a flexible all-fiber QSSLB battery was fabricated by the DIW method and demonstrated a technique to prepare fiber-shape LFP cathode and LTO anode by 3D printing, as shown in Fig. 5 (c). Interestingly, the authors took a unique method to prepare a gel-polymer electrolyte. PVDF-*co*-HFP soaked with 1 M $LiPF_6$ in EC/DEC as gel electrolyte was successfully coated onto the surface of the fiber electrode, enabling a highly integrated all-fiber QSSLB. Both aforementioned works demonstrated fast capacity decay after several cycles and short cycling time: lower than 50 cycles, which is likely mainly due to the low porosity of the polymer electrolyte, although liquid electrolytes were added. Uniform and controlled porosity in battery membranes is a critical parameter for high-rate capability, long-term cycling performance, and dendrite suppression. Therefore, it is necessary to print a high porosity separator/polymer electrolyte to facilitate the Li^+/e^- transport and apply it in the QSSLB design. Dr. Aaron et al reported a controlled, printed porosity electrolyte via a dry phase inversion method in QSSLBs [12a]. The reported electrolyte demonstrated electrochemical performance on par with commercial separator films at a high rate of 5C and maintained a stable cycle performance over 100 cycles at a rate of 0.2 C, as shown in Fig. 5(d) and Fig. 5(e). A key advantage of Aaron's work is that sequential printing gave a rise to a tight and continuous interface between both printed layers, which is beneficial for discharge voltage stability in a flexible energy storage device under mechanical abuse.

Please cite this article in press as: X. Gao et al., Materials Today, (2022), https://doi.org/10.1016/j.mattod.2022.07.016

Another good way to design a seamless electrode/electrolyte interface in solid-state batteries is through the aerosol jet printing technique, which was first demonstrated by the formulation of aerosol jet printable solid polymer composite electrolyte inks [60]. The printed solid-state electrolyte of polyethylene oxide/lithium-difluoro(oxalate) borate/Al_2O_3 (PEO/LiDFOB/Al_2O_3) layer was reported to be smooth, conformal, and conductive enough to be cycled at 45 °C. In addition, a discharge capacity of 162 mAh/g was achieved for the solid-state battery due to the low resistance electrode/electrolyte interface formation by this printing method. However, the safety concerns by operating at high temperatures have limited the application of this system. Hence, realizing solid-state batteries at room temperature is necessary. Recently, a planar flexible full-solid-state lithium-ion battery (FSLB) architecture and layer by layer stencil printing assembly method for fabricating batteries on polyethylene terephthalate (PET) substrate were reported by Zhao et al (Fig. 5(f)) [61]. In Zhao's work, a quasi-solid-state electrolyte with higher ionic conductivity of 2.5 × 10^{-3} S·cm^{-1} at room temperature was achieved. The FSLB assembled with LTO anode and LFP cathode with PEO electrolyte was successfully assembled and demonstrated excellent mechanical flexibility bending radius: under 10 mm was achieved. While the 3D-printing technique applied in batteries has attracted increasing attention in next-generation batteries, there are still some challenges that remain within printing solid-state electrolytes. Additional processing steps are usually needed for electrolyte fabrication, such as solvent evaporation, which hampers the practical application of the printed battery [62]. An elevated temperature DIW method was shown to fabricate hybrid solid-state electrolytes without any additional processing steps by Cheng et al. [23]. As shown in Fig. 5(g), the hybrid electrolyte ink consisted of the solid polymer matrix and a liquid electrolyte which was directly printed onto the electrolyte without the need for any surface treatment of the substrate and post-processing of the electrolyte. Benefiting from the rational design of the electrolyte and electrolyte, the 3D-printed electrolyte presented lower interfacial resistance compared with the conventional method of casting electrolyte onto an electrode. As a result, shown in Fig. 5(h), the batteries assembled with printed electrolytes demonstrated repeatable charge/discharge values and rate performance. This direct fabrication of electrolytes from printed inks at an elevated temperature will open new insight into the design of 3D-printed solid-state batteries for next-generation electronic devices.

Li-S/Se batteries

Despite the wide application of 3D printing in QSSLBs, solid-state lithium-sulfur batteries (SSLSBs) are not yet practical to fabricate via this method. Due to the high theoretical capacity (1672 mAh/g), low cost, and the natural abundance of sulfur, lithium-sulfur (Li-S) batteries have been considered a promising candidate system to overtake LIBs commercially [33,63]. However, there are still some challenges, such as the low electronic conductivity of sulfur, polysulfide shuttle effect, and low operating voltage, that remain to be solved [64]. Also, the liquid electrolyte of Li-S batteries is a serious threat to cell safety [65]. Recently, a work demonstrated a new way to fabricate bipolar SSLSBs that is safe, flexible, and aesthetic [13]. Fig. 6(a) illustrates the stepwise fabrication procedure for the UV curing-assisted, printed bipolar SSLSBs, where two gel-electrolyte based on ethyl methyl sulfone (EMS) and tetraethylene glycol dimethyl ether (TEGDME) were used to address grain boundary resistance of conventional inorganic solid electrolyte as well the polysulfide shuttle effect in SSLSBs. Moreover, the bipolar SSLSBs featured an in-series connection and in-plane connection, as illustrated in Fig. 6(b) upper and bottom, respectively. The SEM images of the printed bipolar SSLSB further demonstrated that unit cells were connected in-series without delamination and cracks. Both reported cells delivered normal charge/discharge behavior in the first cycle (Fig. 6c). These cells also showed a similar cycling performance at a current density of 0.1C, as shown in Fig. 6(d). This is the first reported work to study bipolar SSLSBs with both in-series and in-plane configurations. Nevertheless, the bipolar cells in the reported work just run 50 cycles with discharge capacities around 850 mAh/g, which is lower than other SSLSBs reported at the same current density [66]. Moreover, the sulfur loading in this work is just 0.5 mg cm^{-2}, which cannot meet the requirement of high-energy–density SSLSBs [67]. Therefore, a high mass loading electrode with good cycling performance is necessary for solid-state batteries.

Quasi-solid-state lithium selenium batteries (QSSLSEBs) have attracted more and more attention due to the higher electronic conductivity of 1 × 10^{-5} Sm^{-1} than that of the sulfur element, and comparable volumetric capacity to Li-S batteries (3253 mAh cm^{-3} *vs* 3467 mAh cm^{-3}), and shuttle-free during charging/discharging [68]. However, both poor lithium-ion migration in thick Se electrodes and Li dendrite growth hamper the current density as well as Se mass loading, resulting in low energy/power density. Our group recently proposed ultra-high-energy/power density QSSLSEBs by employing 3D-printed carbon nanotube (CNT) interlayers with high Se loading cathode [69]. As illustrated in Fig. 6f, from a mechanism standpoint, (1) Li dendrite growth was suppressed by 3D-printed CNT interlayers; (2) the combination of the electrode and polymer electrolyte reduced the interfacial resistance, and (3) the 3D-printed Se cathode with polymer infusion facilitated Li-ion transport. Accordingly, the QSSLSEBs delivered excellent cycling stability and remarkable rate performance (Fig. 6f, Fig. 6g).

3D-printed solid-state batteries

Oxide-based solid-state electrolyte

Oxide-based solid-state electrolytes are also very popular materials for batteries due to their high mechanical strength, high chemical stability, large specific surface area, as well as excellent electrical and thermal properties, such as garnet-type $Li_7La_3Zr_2O_{12}$ (LLZO) [70]. However, one bottleneck is the poor contact between electrolyte and electrode, thereby leading to low interfacial resistance. Recently, Dennis et al reported a technique to decrease full cell resistance by using 3D printing to optimize the electrolyte structure [12b]. In this case, LLZO solid electrolyte ink was printed and sintered, revealing thin, nonplanar, and intricate architectures. After processing, the part was ready for electrode infiltration to complete battery assembly, as shown in Fig. 7a. The asymmetric cell of Li|3D-printed LLZO|Li was employed to demonstrate the efficacy of this printed electrolyte. The printed electrolyte demonstrated the ability to suppress lithium dendrite and further

Please cite this article in press as: X. Gao et al., Materials Today, (2022), https://doi.org/10.1016/j.mattod.2022.07.016

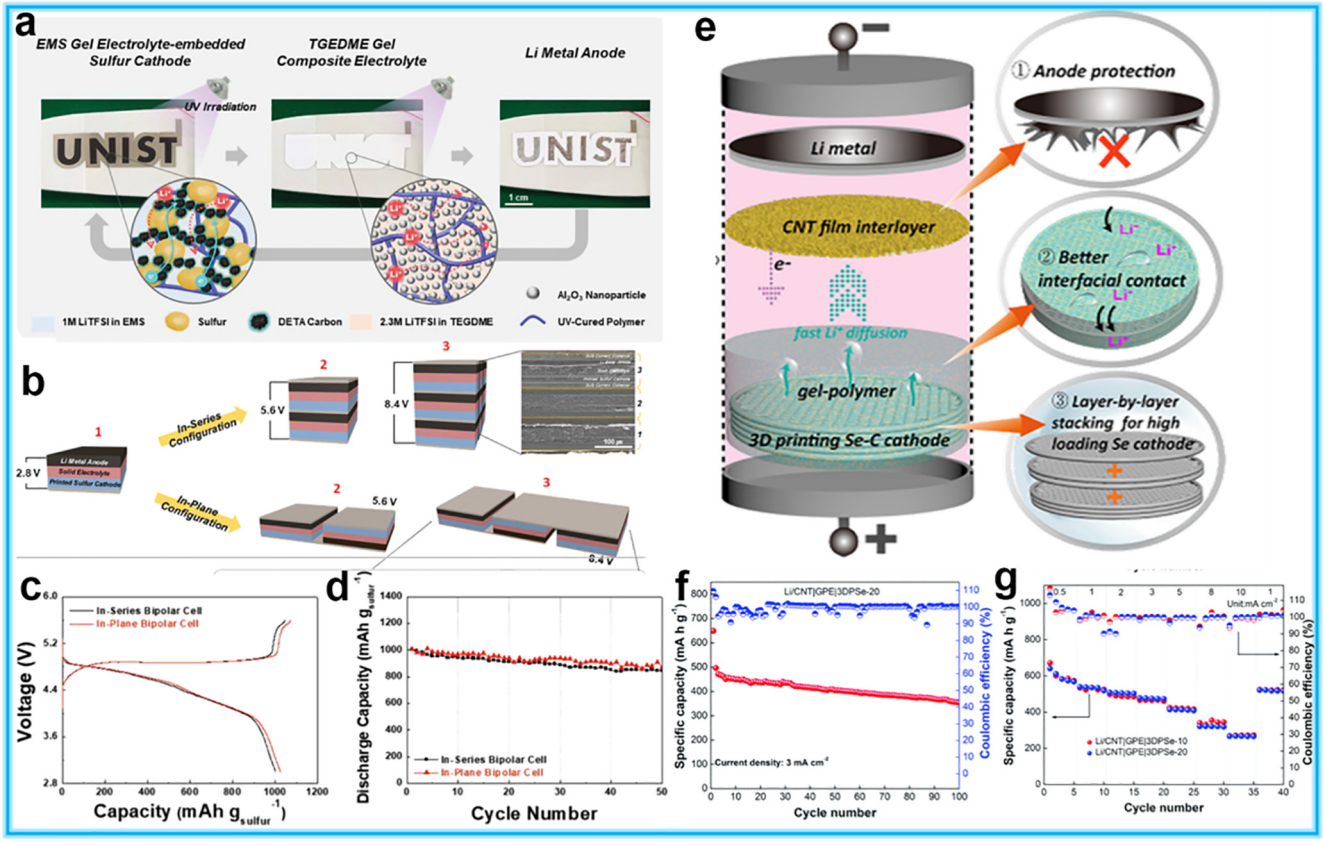

FIGURE 6

(a) Schematic of printed bipolar ASSLBs directly fabricated through UV curing-assisted stepwise printing process. (b) Schematic representation depicting the fabrication procedure of the printed bipolar ASSLSBs, along with an SEM image (in-series configuration). (c) Charge/discharge profiles at the 1st cycle and (d) cycling performance of the printed bipolar ASSLSBs (2 cells connected) at a current density of 0.1C. (e) Schematic overview of an ultra-high energy/power density QSSLSEB with a 3D printed Se cathode. (f) Cycling performance of the Se QSSLSEB at a 3 mA cm^{-2} current density, (g) Rate testing of the Se QSSLSEB.

improve the full cell energy/power density. However, the reported design of flat pellets, without any additive material, presents poor flexibility in the electrolyte, which greatly restricts their scalability and potential for use in flexible electronic devices. Polymer electrolytes play an important role in this system due to the capability of binder and separator membrane. Dr. Lee's group proposed a new class of printable solid-state batteries where the UV-cured (ETPTA) polymer and high boiling point electrolyte, played a key role in achieving the printing process [19a]. A flexible electrolyte membrane based $Li_{6.75}La_3Zr_{1.75}Ta_{0.25}O_{12}$ (LLZTO) garnet-electrolyte, joined together without gaps by styrene-butadiene copolymer (SBC) and 3D printed, was recently reported by Dr. Hu's group (Fig. 7b) [71]. The LLZTO garnet chips functioned as fast lithium-ion transport channels while the SBC grid served as a deformable buffer to decrease the stress transferred to the chips. As a result, no ion-diffusion-limited process (Warburg impedance) was seen in Fig. 7c due to deposited Li metal on both sides of the composite electrolyte. This tile-and grout-designed electrolyte composite membrane possessed high flexibility and could be readily bent into a small radius without cracking. Such a design presents a new insight for future printed flexible solid-state electrolytes.

Hybrid solid-state electrolyte

Benefiting from the combination of garnet-based electrolyte and polymer electrolytes, another class of electrolytes is the hybrid electrolyte. A 3D bi-continuous ceramic solid-state electrolyte, $Li_{1.4}Al_{0.4}Ge_{1.6}(PO_4)_3$ (LAGP), and non-conducting polymer (epoxy polymer, polypropylene) micro-channeled electrolyte were printed as reported by Bruce's group [72]. As illustrated in Fig. 7d, the LAGP ceramic channels provided continuous, uninterrupted pathways, possessing high ionic conductivity between electrodes, while the polymer channels increased the mechanical properties from that of ceramic alone. The best ionic conductivity of 1.6×10^{-4} S cm^{-1} at room temperature was shown by the gyroid LAGP-epoxy electrolyte polymer in Fig. 7e. Therefore, optimizing the mechanical and electrical properties of solid-state electrolytes can mitigate the lithium metal/solid-state electrolyte interface. However, the aforementioned work did not demonstrate the benefit of a hybrid electrolyte at the cathode. Therefore, to enable the seamless architecture/electrical connection, a fabrication of a printed solid-state bipolar lithium-ion battery through an in-series printing process was proposed by Sang-Young Lee's group [19b]. In that work, the LTO anode paste was printed on the top of the Al metal electrode of the crystalline Si photovoltaics (c-Si PV) module by stencil printing, and then exposed to ultraviolet (UV) irradiation for a short time of less than 30 s. The solid-state electrolyte-based ETPTA/1M $LiPF_6$ in EC/PC/Al_2O_3 nanoparticles, with a weight ratio of 7.5/42.5/50, was then printed on the top of the LTO anode using the same method that enabled the formation of a thin layer electrolyte

Please cite this article in press as: X. Gao et al., Materials Today, (2022), https://doi.org/10.1016/j.mattod.2022.07.016

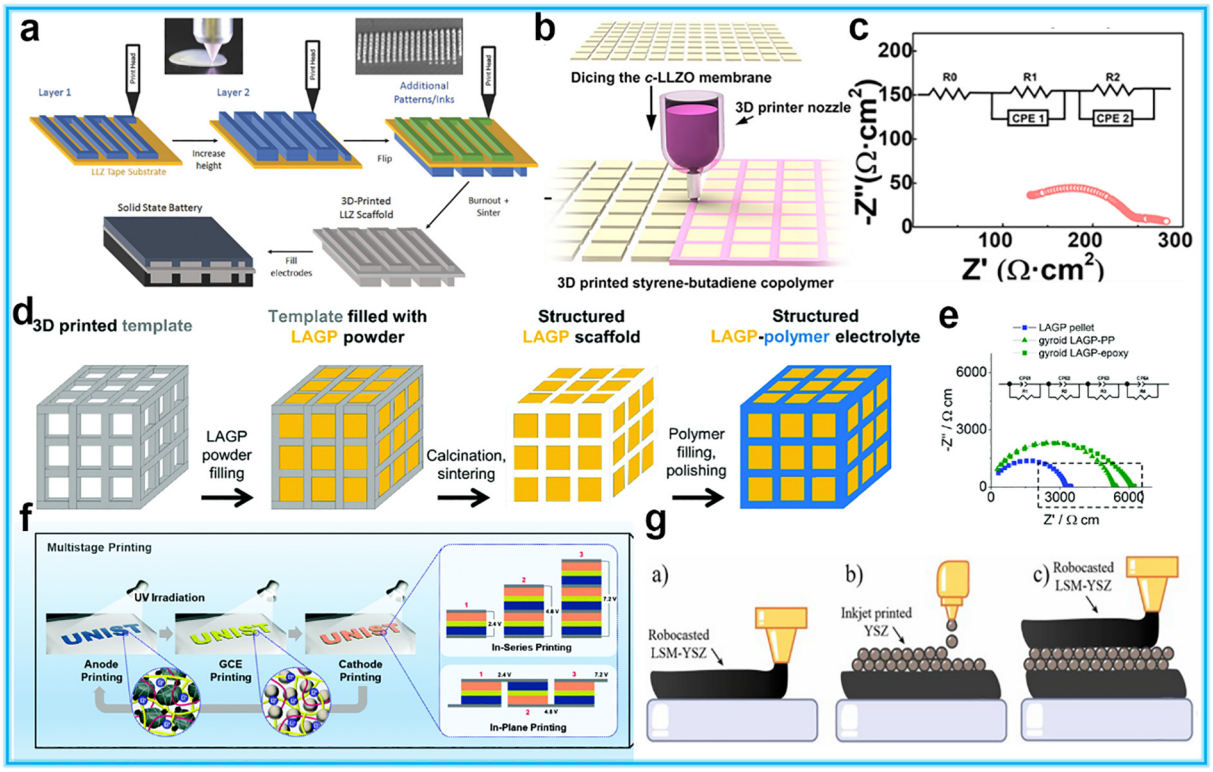

FIGURE 7

(a) Schematic illustration of the process to 3D-print solid electrolyte structures. (b) The fabrication process of flexible composite electrolyte. Styrene-butadiene copolymer (SBC) ink was printed to bind the neighboring c-LLZO chips together. (c) EIS profile of the printed electrolyte at room temperature. (d) Schematic illustration of the templating procedure used for the synthesis of structured hybrid electrolytes with a cube microarchitecture example. (e) Nyquist plots of the symmetric cell by employing a LAGP pellet, a gyroid LAGP-PP and a gyroid LAGP-epoxy electrolyte. (f) Schematic of the flexible/shape-versatile bipolar cells prepared via the UV-assisted multistage printing process. (g) Schematic representation of the hybrid printing process to produce the symmetrical cells.

on the LTO anode. The LCO cathode was then printed directly on the electrolyte/LTO unit and exposed to UV irradiation. Meanwhile, another identical battery was introduced on the top of the as-fabricated battery unit cell via the same printing process, resulting in the fabrication of a bipolar stacked lithium-ion cell. This rational design can be beneficial for solving the issues of interfacial contact resistance. Lee's group also proposed a new class of flexible/shape-versatile bipolar SSLBs with an LCO cathode, gel-polymer electrolyte, and LTO anode using UV curing-assisted multistage printing technique [12c]. As shown in Fig. 7f, two different batteries based on in-series printing and in-plane printing were fabricated. For cells with an in-series configuration as a function of cell numbers from 1 to 3, the charge/discharge profiles demonstrated that, as the cell number increased, the working voltages elevated from 2.4 V (mono cell) to 5.4 V (two cells) to 7.2 V (three cells). The charge/discharge profiles of using two mono cells connected in-series or in-plane reflected normal charge/discharge behavior and good coulombic efficiency (~98%). Also, there was no reported obvious difference in the profiles, which suggested the versatility and effectiveness of the printing process with UV-assisted technique in the work. Such a technique for bipolar cell fabrication holds great promise for the development of next-generation solid-state batteries. Moreover, 3D printed symmetrical cells were shown by a robocasting and inkjet printing hybrid technology, followed by a co-sintering step. Fig. 7g describes the hybrid printing process for manufacturing the symmetrical cells [13c]. The process can be divided into three steps: (a) deposition of the supporting bottom electrode of $La_{1-x}Sr_xMnO_3$ – Yttria Stabilized Zirconia (LSM-YSZ), followed by curing; (b) inkjet printing of the YSZ electrolyte on top of the bottom electrode; (c) robocasting of the top LSM-YSZ layer on the inkjet-printed YSZ and subsequent curing. The fabrication of the cells following these steps made it necessary to formulate and characterize the slurries for the deposition of the LSM-YSZ electrodes via robocasting and of a YSZ ink for the deposition of the electrolyte. This study presents the fabrication of complete cells with self-standing electrodes combined with inkjet-printed electrolytes and their co-sintering in one step.

Cutting edge in printing technologies and future trends

The field of 3D printing has experienced rapid development and growth in recent years. As a result, various new printing technologies have begun to emerge in both academic and industrial applications. In this section, we review the current landscape of cutting-edge 3D printing technology including powder-based printing techniques, the use of electric fields, nanoscale printing techniques, and 4D printing. Within, we highlight the working principle and suggest applications for lithium battery fabrication.

Please cite this article in press as: X. Gao et al., Materials Today, (2022), https://doi.org/10.1016/j.mattod.2022.07.016

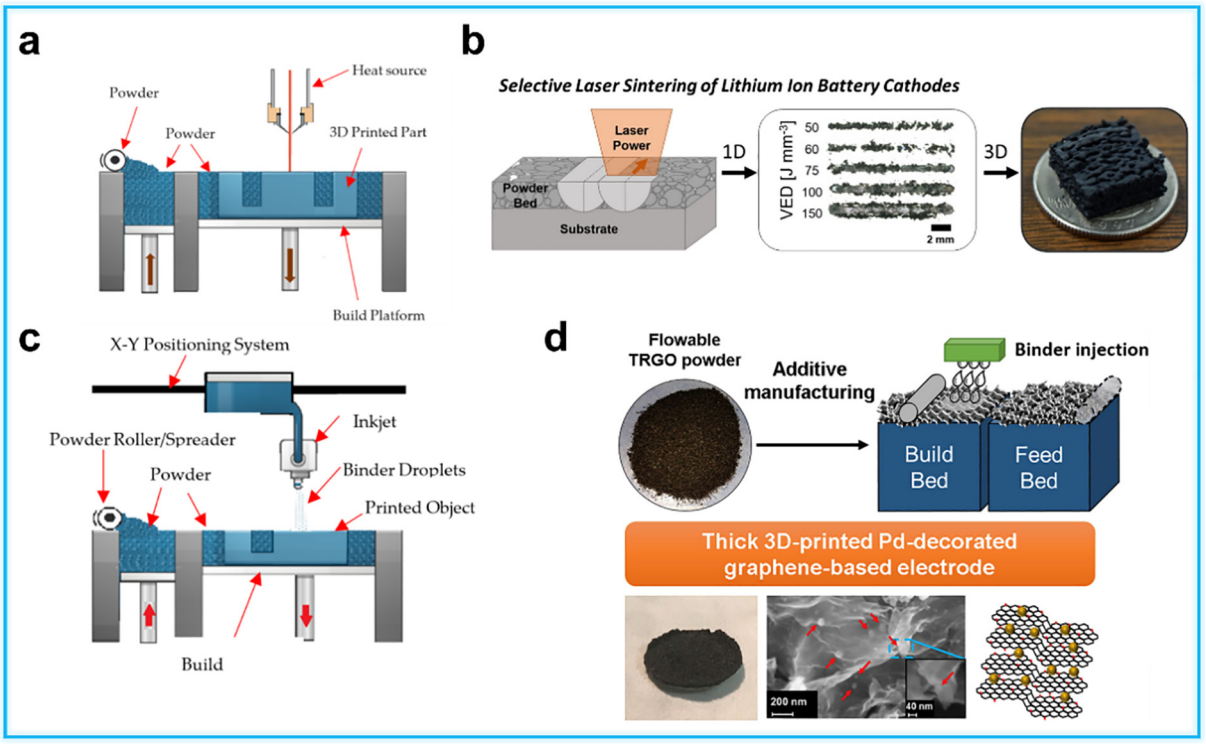

FIGURE 8

(a) Schematic outline of powder-based Selective Laser Sintering and Selective Laser Melting set-up (SLS and SLM). (b) Graphical representation of SLS printing process of lithium nickel cobalt aluminum oxide (NCA) cathode, printed NCA of different widths as a function of volumetric energy density, and final printed cathode. (c) Schematic outline of Binder Jetting printing (BJ). (d) Graphical process depicting BJ printing of thermally reduced graphene oxide infused with palladium particles, the final printed part, and observed crystal structure.

Powder-based sintering, melting, and fusion

Powder-based 3D printing is an additive fabrication process by which each layer is composed of a multitude of powders that have been joined together [74]. This printing method is rapidly being adopted and changing the aerospace, dental, and metal processing industry [75a]. The method by which the powders have been joined dictates the classification of the printing process. The generally accepted classifications are powder sintering, melting, and binder-based joining. Powder sintering and powder melting are set up almost identically, as outlined in Fig. 8(a) [75b].

In the sintering process, coined Selective Laser Sintering (SLS) printing, a bed of powders lay on the printing substrate. A high-power (hundreds of watts) laser travels over the packed particles in a pattern dictated by the inputted and sliced 3D model [76]. The powders, typically a metal, ceramic, or polymer are heated to an appropriate temperature to invoke local fusion of particles through molecular diffusion. After sintering the surface 2D slice, the printing platform is moved down, fresh powder is overlayed, and then processing of the next layer starts. In addition to metal powders, SLS printing can also print polymers such as polycaprolactone (PCL) and polyamide (PA) [20].

However, in the melting process, known as Selective Laser Melting (SLM), packed particles on the printing substrate are exposed to a similar high-power laser. Laser travel speed and intensity are adjusted such that the particles exposed to the laser photons will fully melt in an approximately homogenous manner [77]. The resulting part printed by SLM will have a higher density and fewer defects related to porosity. A similar melting method is Electron Beam Melting (EBM). As the name suggests, rather than use a photon-based laser as in SLM, the EBM process will melt particles with a high-power electron beam under a vacuum [78]. EBM is often applied in applications where high resolution is a secondary requirement and high speed of printing is the primary requirement. Another printing technology that uses either similar lasers to the SLM or an electron beam such as in the EBM method is the Directed Energy Deposition (DED) printing technique. In the DED process, wire or powder material is fed to an extrusion nozzle. At the end of the nozzle, a source of heat is provided by either laser, electron beam, or plasma arc [79]. The DED process affords users the ability to print with low amounts of waste raw powder and high fabrication speed. However, complex geometry is often not feasible to be printed by the DED process due to the inherent lack of support structures.

Another common printing method is Binder Jetting (BJ) which is a printing method that requires the local dispersion of binding agent powders to join them together, as visualized in Fig. 8(c) [75b]. BJ printing was developed at the Massachusetts Institute of Technology (MIT) in 1993 as a rapid prototyping technology [16]. In BJ printing, powders are first spread on the build platform and then selectively joined into a patterned layer by depositing a liquid binder through a print head, which follows the printing path set by the original inputted and sliced 3D model [80]. After a desired 2D pattern is formed, the platform lowers, and a fresh layer of powder is spread. This process is repeated. In the final step, the unbound powder will be removed to yield the final product(s). The internal structure can be con-

Please cite this article in press as: X. Gao et al., Materials Today, (2022), https://doi.org/10.1016/j.mattod.2022.07.016

trolled by altering the amount of deposited binder. Factors that determine the quality of final products are powder size, binder viscosity, interactions between the binder and powder, and the binder deposition speed. The key advantages of this technology are the flexibility of material selections as there are fewer material restrictions, given that the powders do not require melting or sintering. However, BJ printing requires a mandatory post-processing step to form the final part which requires the decomposition and removal of the binder agent, sintering of the base material, and infiltration of another material to take the place of the pores from the removed binder.

Powder-based printing methods are still new to the field of energy storage, especially for battery fabrication. Due to the high-temperature nature of the sintering and melting process, only high-temperature powder materials are generally suitable as the raw material input. Hence, this eliminates the option of directly using delicate materials and some structured nanomaterials as the raw material. However, the use of SLS and BJ has been introduced in electrode design. Ibrahim et al. used SLS printing to fabricate a highly porous, electrically conductive stainless-steel scaffold. Through modification of scan speed and laser power, tunable porosity was developed as a pathway for fabricating scaffolds with up to 15.61% porosity and with an associated electrical conductivity of 1.8×10^6 S/m [81]. A further development was introduced by Marcel et al. who demonstrated the application of SLS to fabricate lithium iron phosphate cathodes using polypropylene, mixed with $LiFePO_4$, carbon black, carbon nanofibers, and paraffinic oil. Maruel and co-authors compared the SLS printed electrode against the performance of an FDM printed electrode with the same material composition, only processed into a filament for the FDM printing process [82]. More recently, Acord et al. used SLS to fabricate a binder-free NCA cathode as a feasibility study (Fig. 8(b)). The printed electrode with a thickness of 100 μm could be processed without a binder into a solid part, with an observed dual ordered and disordered rock salt crystal structure. However, significant cracking and void formation was observed [83]. In a different approach, Azhari et al. demonstrated the use of BJ to print thermally reduced graphene-based electrodes for supercapacitors (Fig. 8(d)). After BJ printing and sintering, Azhari and co-authors infiltrated the electrode with palladium nanoparticles [84]. The resulting BJ printed supercapacitor could retain 80% capacity over 1000 cycles.

Powder-based 3D printing has a wide breadth of applicability for battery development, especially for solid-state systems. By nature, much of the synthesis of solid-state batteries requires the processing of powders in the electrolyte and cathode. Each powder-based printing method has potential for application in not only the fabrication and formation of battery components, but to change modify the chemical structure and introduce new synthesis pathways through the different joining mechanisms of melting, sintering, and joining.

Electric field application in printing

The most prevalent use of electric fields in manipulating standard 3D printing processes is the technique known as Electrohydrodynamic inkjet printing (E-jet printing), as visually illustrated in Fig. 9(a) [85a]. In E-jetting, an electric field is applied to a

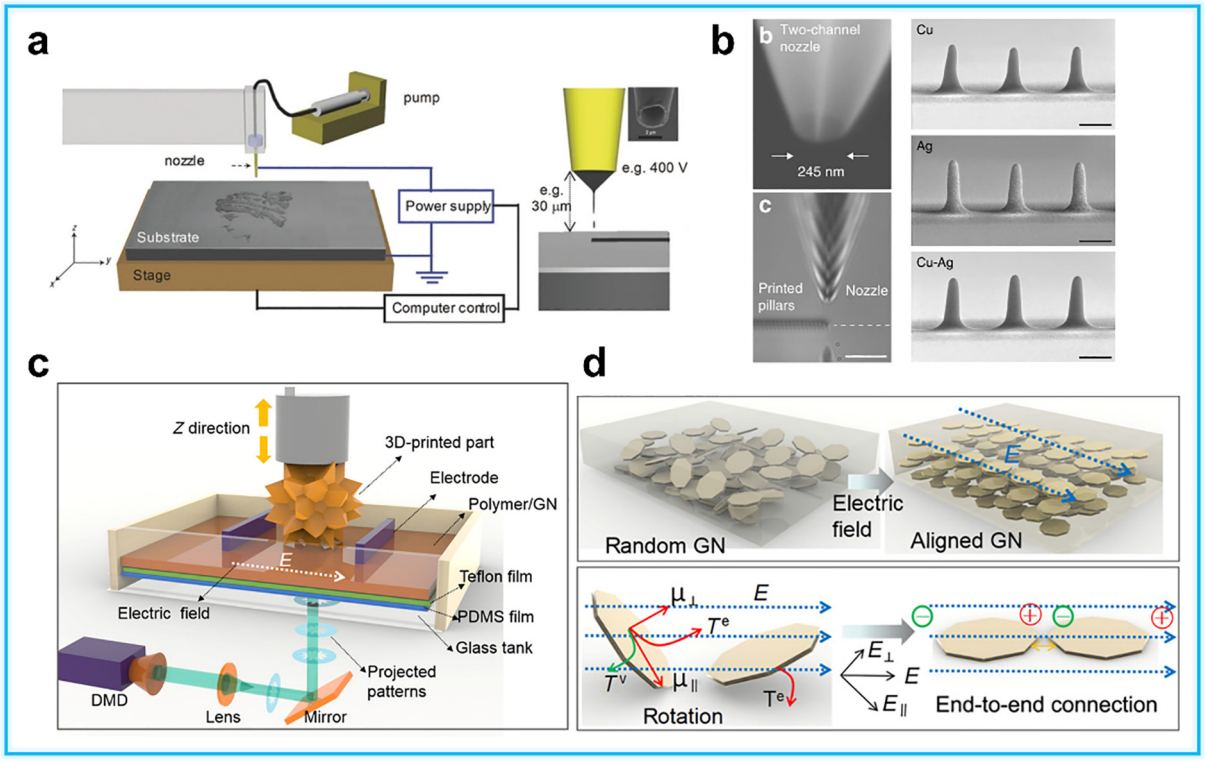

FIGURE 9

(a) Schematic demonstration of the Electrohydrodynamic jet printing (E-jetting) process. (b) Freestanding copper, silver, and copper-silver alloys printed by E-jetting. (c) Experimental 3D-printing set-up of photosensitive resin-infused by graphene nanoplatelets with orientation controlled by an electric field. (d) Alignment mechanism and schematic visualization of graphene nanoplatelets under electric field.

Please cite this article in press as: X. Gao et al., Materials Today, (2022), https://doi.org/10.1016/j.mattod.2022.07.016

reservoir of polar liquid ink which causes a build-up of ions and eventually the deposition of a single drop of printing ink onto the substrate once the surface tension force at the nozzle is overcome [85]. Through this mechanism, various polar liquid inks can be deposited at resolutions in the sub-micro and nanometer range. This technique is widely popular in the medical field, where applications have included 3D tissue scaffolds, cancer drug-delivery devices, and patterning DNA ink [86–88]. An advanced use case of E-jet printing is enabling multi-metal printing and the fabrication of sub-micron scale metal alloys when depositing two metal inks at the right temperature and relative composition (Fig. 9(b)) [89]. In 2019, Reiser et al. demonstrated this concept by printing varying 3D configurations of Cu, Ag, and Cu-Ag alloys through a single nozzle with two different material feed (Cu and Ag). Along similar lines, the unique deposition mechanism of E-jetting can enable fine control of the orientation of printed material. Lee and co-authors demonstrated that it is feasible to align Ag nanowires perpendicular to the printing motion of an E-jet printing nozzle [90]. This highly controllable and high-resolution printing process that can deposit various forms of ink, especially functional inks, opens the possibility of locally adjusting surface properties of materials, in addition to fabricating small-scale functional devices. In battery application, this is a technique that would be well suited to modifying interface behavior and can have tangible applications when combined with existing functional energy storage materials.

The application of electric fields extends far beyond the E-jet printing process. In all forms of 3D printing, electrical fields can be directly used to modify the orientation of constituent components in the printed part. In particular, printed inks or molten materials are viable states for changing the orientation of nanomaterials through the application of electric fields. Chen et al. demonstrated the use of a custom-DLP printer set-up with a rotating and movable printing platform situated between two external electrodes that applied a direct current electric field on multi-walled carbon nanotubes in the printing resin [91]. The resulting printed part under the applied electric field yielded significantly superior mechanical properties in terms of maximum tolerable load and fracture resistance. Yang, et al. proceeded to demonstrate a similar concept applied to align graphene nanoplatelets to act as a mechanical barrier with the implied application for the medical, military, and sports industries (Fig. 9(c), (d)) [92]. Similar applications can be obtained by the utilization of magnetic fields to align nanomaterials such as carbon nanotubes (CNTs). As CNTs require a catalyst nanoparticle to grow, it is practical to use a magnetic field to modify the orientation of a ferromagnetic catalyst nanoparticle [93]. Although magnetically aligned CNTs have been demonstrated in the literature [94–96], there has yet to be a demonstration of magnetic fields to align CNTs in conjunction with 3D printing. However, Kokkinis et al. demonstrated the applicability of using magnetic fields to align alumina platelets in DIW ink [97]. Through changing the position and orientation of the magnet, various physical structures were constructed inside the printed part.

Nanoscale printing

3D printing as a fabrication technique has the advantage of enabling fine microscale control of geometry. Improved printing resolution requires finer control of the *X*–*Y* and *Z* movement, as well as the deposition technique, whether that is a nozzle like in FDM or DIW or the width of the laser in SLM or SLA. Recent development in improving the fidelity of the instruments inside printers has helped make sub-micrometer resolution printing possible. Among the most powerful and high-resolution printing techniques is the Two-Photon Polymerization (2PP or TPP) printing technique. The generalized working principle is very similar to that of SLA printing, however, in TPP the laser is switched to a femtosecond laser which is focused into a vat of photopolymers that have photoinitiators capable of absorbing two photons simultaneously. As a result, TPP is capable of printing parts at resolutions beyond the theoretical diffraction limit [98]. A typically expected printing resolution for TPP printing is as low as 100 nm. For these reasons, TPP has and still is being met with great interest from various fields. For battery applications, there is significant promise in the ability to create nanoscale features with a high degree of control. Such as the design of a high mass loading cathode by employing nanoscale printing to facilitate Li^+/e^- transport, and then further increase the energy density of Li batteries. Potential use cases could include the fabrication of complex electrolyte structures, the combination of polymer electrolyte and oxide-based electrolyte to reduce interfacial resistance. However, the major challenge to address is how to use additional functionality to the TPP process without inhibiting the two-photon photoinitiator absorption mechanism.

4D printing

The ability to print in three-dimension sparked significant interest and change in traditional manufacturing processes such as in the metals manufacturing, aerospace, and footwear industry. Four-dimensional printing, 4D printing, offers a similar prospect. Conceived in 2012, the concept of 4D printing is to make 3D parts change concerning time or external stimulus [99]. The end goal is for 4D printed parts to have the ability to respond to external change, ideally in the capacity of self-repair, self-assembly, or endowing new functions dependent on the environment [100]. The general working principle is dependent on the specific solution used.

To enable 4D printing, the careful selection, design, and programming of 4D materials is critical, in addition to careful 3D printing of the desired part. In any 4D printed part, there is a requirement for external stimuli such as temperature, mechanical stress, electricity, magnetic fields, change in moisture, pH, or time to invoke a physical change in the material. Through careful design, positioning, and calculations of the desired response such as deformation, the 4D printed part will change accordingly. Although there is a multitude of 4D materials, there are four general classes of materials receiving significant interest. (1) Shape Memory metal Alloys (SMAs): materials that will restore their original shape irrespective of the deformation they experienced. This is possible through careful selection of alloy chemical composition to allow for phase change and restoration of shape with specific heat treatment paths, as summarized in Fig. 10(a) [101]. (2) A similar class of 4D materials is Shape Memory Polymers (SMPs). Similar to SMAs, SMPs will withstand large deformation and return to their original shape when heated typically about their glass transition temperature (Fig. 10(b)) [101b].

Please cite this article in press as: X. Gao et al., Materials Today, (2022), https://doi.org/10.1016/j.mattod.2022.07.016

However, SMPs are capable of multiple configurations that can be activated at varying temperatures, unlike SMAs which are typically limited to just a recoverable original configuration [102a]. However, both of SMAs and SMPs require a change in temperature as stimuli. (3) Hydrogels are a widely popular class of materials that respond typically to water via volume change, as demonstrated in Fig. 10(c) [102b]. However, hydrogels are also programmable to respond to change in pH [103]. (4) Composites, typically a long fiber component embedded in a soft host matrix material are also capable of being programmed to act as a 4D material. Among the most common 4D composites are the CNT composites, which typically respond to electrical stimuli or hydrogel composites as shown in Fig. 10(d) [104].

While 4D printing is still a relatively new area, there is significant promise for what where its application could lead. In an application in batteries, this could take the shape of using 4D printed electrodes or even a 4D printed battery case to accommodate volume change during cycling. Small 4D printed additives in electrodes could be used dynamically to promote a higher ionic conductive pathway or an insulative pathway. 4D printed interlayers could be designed to selectively allow diffusion of specific ions. However, it is important to recognize that 4D printing builds directly on top of the 3D printing technology, by design. Hence, there is of great importance to fully develop our 3D printing capabilities in conjunction with pursuing the development of 4D printing.

Post-print processing techniques

Despite the rapid development in recent years, 3D printing is far from an end-to-end process. Post-processing of some form is nearly always required, regardless of the printing technique. In this section, we highlight the common post-printing processes, the underlying rationale, and the working mechanisms. In particular, we cover the post-processing of all common printing techniques including resin-based, powder-based, and ink-based printing. The relevance of discussing post-printing processing is to highlight the methodology to ensure the highest dimensional accuracy possible.

Resin and powder post-processing techniques

Resin-based 3D printing requires three major post-processing steps. The first is the removal of any excess resin from the part. Common techniques in practice include the use of ultrasonication or a physically abrasive medium to remove residual resin, in conjunction with large amounts of ethanol or isopropanol. The second requirement is the removal of all support material. As the just-printed part in resin-based printing is not fully polymerized, it is apt to remove any support structures. Third, post-printing curing is required by exposing the printed part to UV light treatment, ideally with a 405 nm wavelength light for no more than a few hours [105]. Using a standardized post-processing procedure across all individual experiments is statistically relevant. Ammoun et al. demonstrated errors up to 0.18 mm can occur when simply using different lengths of time and settings for ultrasonication, UV light treatment, and length of time rinsed. With certain SLA, DLP, and TPP processes printing at a resolution in the sub-micrometer range, standardizing post-processing is significant for ensuring the highest dimensional accuracy. For battery application, careful post-processing of resin-based prints is required to ensure consistency and accuracy of the printed components. With most battery components fabricated in the micrometer range, millimeters of dimensional change due to processing is not acceptable.

Powder-based 3D printing is dependent on the specific process but there are two shared post-processing requirements common among all techniques [106]. First, to ensure dimensional accuracy, remove the 3D printed part from the powder bed or the printing environment and use a physical method to remove excess powder, or use a tumbler to jolt the excess powder off the printed part. A follow-up cleaning of the sample should be conducted with a pressurized gas gun to ensure thorough removal of residual material. The second is either further sintering and infusion for BJ processes or surface finishing for most other powder-based printing. A non-required post-processing option but a highly standardized one in any industry requiring the printed component to bear loads is the use of isostatic pressing (IP) or hot isostatic pressing (HIP) to remove porosity and densify the part. The processing parameters for IP and HIP are dependent on the material printed but also on the final part requirements [107]. Most powder-based 3D printing is still relatively new in an application for batteries; however, porosity is not always necessary to be eliminated. Depending on the application, skipping post-processing or inducing larger porosity by choosing faster laser travel speeds, larger raw powder size, or changing other printing parameters could be desired.

Ink-based post-processing techniques

Ink-based 3D printing such as DIW is highly dependent on the use scenario. The parameter of interest is moisture: in some applications such as biomedical, moisture is critical [108]. However, in battery design, specifically lithium batteries, water is highly undesirable, and therefore must be removed. While heating at elevated temperature is the fastest path, it is also the most likely to cause structural deformation of the printed electrode. Common techniques are to either dry at ambient temperatures or to freeze dry and sublimate the water from the electrode [109].

Filament post-processing techniques

In filament 3D printing, the critical post-processing requirement is to remove all the support structures and polish the surface of the part. The extent of the surface polishing is highly dependent on the application. However, due to FDM's popularity, there have been several post-processing paths have been developed. Sand blasting or sanding with paper is an abrasive technique that removes dimensional inaccuracies [110]. Sanding should be carried out with low grit and gradually transition to fine grit for optimal results. However, this is purely a cosmetic post-processing path. Acetone dipping is a common cosmetic post-processing path as well, which will smooth the inconsistency between layers and create the appearance of a high-resolution part. However, acetone baths are known to cause a decrease in tensile load-bearing strength [111]. A similar effect can be done by using acetone or ethyl acetate as a vapor source and enveloping the printed part in a confined environment [112].

Please cite this article in press as: X. Gao et al., Materials Today, (2022), https://doi.org/10.1016/j.mattod.2022.07.016

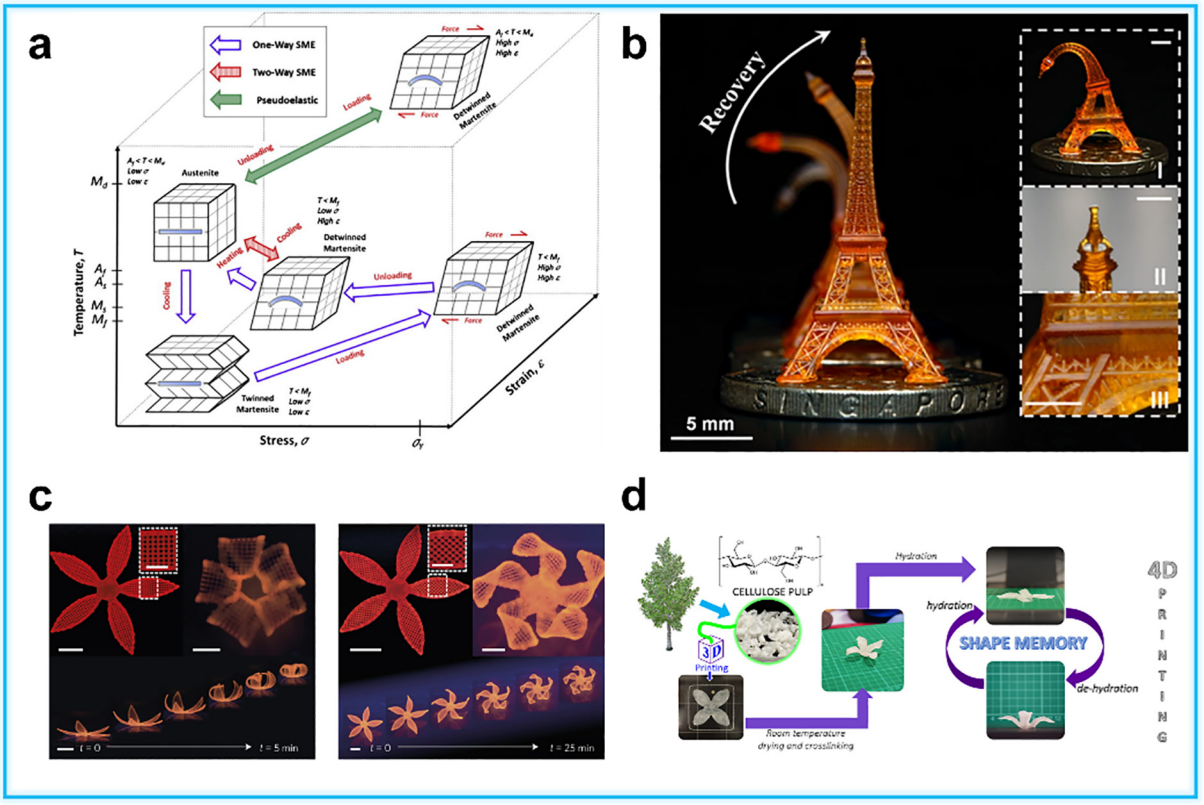

FIGURE 10

(a) Different phases of carbon steel Shape Memory Alloys demonstrate the ability to recover from deformation given proper heat treatments. (b) Shape memory polymer printed into the shape of an Eiffel tower, demonstrating full geometric recovery capability upon heating after an initial deformation at room temperature. (c) Hydrogel printed flower demonstrating folding of petals after exposure to water which induces swelling. (d) Carboxymethyl cellulose hydrocolloid matrix infused with cellulose fibers forms a composite flower that can flatten and recover the original flower shape depending on the level of hydration provided by the environment.

Conclusion and perspective

Conclusion

In this review, we have reviewed the applications of printing techniques in batteries from liquid- to solid-state batteries. For the liquid-state battery systems, the cathode, anode, and micro-battery designs fabricated via 3D printing are discussed. Analysis of 3D printing's role in improving electrochemical performance is provided. Thick cathodes with high mass loading are also highlighted and reviewed in this paper. In addition, the lithium metal anode-based 3D printing progress and techniques to suppress lithium dendrite growth, such as fabricating 3D hosts and melting lithium metal to obtain a 3D lithium anode to further guide lithium deposition, have been also discussed in this review. More importantly, we discuss the wide application of 3D printing for enabling the tunable design of devices, like micro-batteries or design of high energy density batteries, etc. In later sections we discussed and reviewed solid-state batteries-based 3D printing methods, featuring systems such as printing oxide-based electrolytes, polymer electrolytes, and hybrid solid electrolytes. Based on design principles, ionic conductivity and air stability of the solid electrolytes are directly chosen as two important parameters for improvement through 3D printing. Moreover, we discuss 3D printing's viable application to address the critical interfacial resistance of electrodes and electrolytes in SSLBs. Due to the ability of 3D printing to create seamless electrode/electrolyte interface design, there is a great application for 3D printing SSLBs. We then share recent advances and progress in the areas of different electrolytes, and battery systems, and share some important insights. We then transition the discussion to the cutting edge of the 3D printing field and the potential opportunities it creates for the field of battery research. In particular, we highlight the development of powder-based 3D printing techniques, electric fields for modifying the printing process, new nanoscale printing techniques, and the emergence of 4D printing. In each section, we share our outlooks and how each emerging 3D printing technology can impact battery design. In the final section, we reviewed critically and required post-processing techniques for all forms of 3D printing including resin, powder, ink, and filament-based printing. In each post-processing technique, we highlight what parameters are of significance specifically for battery researchers.

Although much progress has been made in manufacturing batteries using 3D printing, there are still numerous challenges that must be addressed before they are widely used commercially. It also has three drawbacks of 3D printing technology applied to Li batteries. The first one is the cost, unlike more conventional techniques like injection molding. Once it can be scaled up to produce a large volume for practical application,

Please cite this article in press as: X. Gao et al., Materials Today, (2022), https://doi.org/10.1016/j.mattod.2022.07.016

such as the 3D-printed electrode and electrolyte, the cost per unit would be increased compared with other methods, such as the blade casting method. The second drawback is the limitation of printed materials. For example, some 3D printing material of choice is plastic. Plastic is preferred as it can quickly and easily be deposited down in melted layers to form the final product. However, plastic may vary in strength and may not be ideal for some components, such as battery electrodes. The third drawback is the long printing time. Depending on printer size and quality, it can take several hours to days to print some batteries' components. The more the work involved with product development, the slower the 3D printers are. Therefore, three directions should be focal points for research efforts for applying 3D printing in battery development.

Perspectives

1: Designing of high-resolution printers and compatible functional ink

A major challenge lies in improving the precision of printers to a level suitable for battery design and application. Current-day printers have accurate printing resolution down to the micro-level, but most cannot yet print functional material at the nanoscale, which could enable control of Li^+/e^- migration. As an example, the design of holes at the nanoscale is a widely accepted way for researchers to improve battery performance. Techniques such as freeze-drying and phase inversion can be employed to form the nano-scale holes. However, they are not fully controllable processes. Furthermore, there exist intrinsic resolution bottlenecks in functional material printing such as the diameter of the powdered materials used. Thus, the design of high-resolution printers and compatible functional ink are both of equal importance to realize the techniques that will greatly improve the application of 3D printing for battery fabrication. This point paves the way for further improving the energy density and power density. Therefore, the design of high-resolution printers and compatible functional ink is one of the most important efforts that will improve the application of 3D printing for battery fabrication. The success of nanoscale printing would open many exciting opportunities and future directions, such as adding functionality to the material by printing the 4D materials, which can change when stimulated by changes in their environment.

2: Developing thick electrodes in combination with 3D printed thin SSEs

Currently, most of the research efforts regarding batteries are focusing on fabricating high mass electrodes and thin SSEs to achieve the goal of high energy/energy density batteries. Recently, extensive works regarding thick electrodes with high mass loading have been studied. Typical works include the design of a thick LFP cathode for LIBs, a sulfur cathode for Li-S batteries, and a Se cathode for solid-state Li-Se batteries through DIW printing [31,48,69]. Moreover, 3D structures of hybrid SSEs with high ionic conductivity and lowered interfacial resistance are also investigated in SSLBs [12c,d]. However, the joint study of these two focuses together has rarely been investigated. With the emergence of 3D printing as a viable electrode and electrolyte fabrication path, more efforts should be considered to design and develop thick electrodes in combination with 3D printed thin SSEs to realize the goal of high energy and high energy density batteries. In particular, thanks to the development of powder-based 3D printing processes, there is now a new viable pathway to fabricating SSEs. We envision that combining 3D printing with electrode and SSE fabrication will open new opportunities in increasing energy density and lowering the cost of SSLBs.

3: Developing functional materials with high cohesion and stability against lithium anode

Finally, the utilization of 3D-printed lithium or alloy metal to guide lithium deposition and address fundamental challenges can bring new functionalities to lithium metal batteries and is an inevitable future research area. For example, the current day design of 3D structured lithium anodes employs 3D printing methods to print 3D hosts, progressing towards the goal of lithium dendrite-free and high-performance lithium symmetric cells [42,73]. Despite the efforts and desire to print 3D lithium metal for lithium metal batteries, the experimental complexity of using lithium metal directly as a printing material is the main factor limiting the development of high-performance lithium metal batteries. The successful design of lithium metal batteries via 3D printing will require the combination of key features such as high-precision printing with nano-scale control, printing material stability at high temperatures, and mastery of the printing process and post-processing. Functional materials with high cohesion and stability against lithium such as carbon inks containing CNTs, or carbon black incorporated into melted lithium metal or alloy feed materials used as reinforcement may be a good starting direction to realize 3D printed lithium metal anodes or alloy metal anodes. By leveraging the strengths of 3D printing, there is great potential to discover new insights into 3D lithium anode design.

Declaration of Competing Interest

The authors declare that they have no known competing financial interests or personal relationships that could have appeared to influence the work reported in this paper.

Acknowledgements

This research was supported by the Natural Science and Engineering Research Council of Canada (NSERC); the Canada Research Chair Program (CRC); and the Canada Foundation for Innovation (CFI), and Western University.

References

[1] (a) M. Hannan et al., Renew. Sustain. Energy Rev. 69 (2017) 771–789;
(b) S. Xin, Y.-G. Guo, L.-J. Wan, Acc. Chem. Res. 45 (2012) 1759–1769;
(c) F. Wu et al., Electron Energy Rev. 4 (2021) 382–446;
(d) H. Li et al., J. Am. Chem. Soc. 142 (2020) 2012–2022;
(e) C. Ye et al., Matter 2 (2020) 323–344;
(f) X. Yuan et al., Electron. Energy Rev. 4 (2021) 1–34.
[2] (a) T. Jin et al., ACS Appl. Mater. Interfaces 11 (2019) 17333–17340;
(b) J. Nelson et al., J. Am. Chem. Soc. 134 (2012) 6337–6343;
(c) M. Balaish et al., Nat. Energy 6 (2021) 227–239.
[3] (a) L. Wang et al., Joule 3 (2019) 2086–2102;
(b) Q. Zhou et al., Adv. Mater. 31 (2019) 1902029;
(c) J. Cai et al., Adv. Mater. 32 (2020) 2005967;
(d) F. Zhang et al., ACS Sustainable Chem. Eng. 9 (2021) 6097–6106.
[4] (a) T. Wallin, J. Pikul, R. Shepherd, Nat. Rev. Mater. 3 (2018) 84–100;
(b) T.S. Wei et al., Adv. Mater. 30 (2018) 1703027;
(c) C. Panwisawas, Y.T. Tang, R.C. Reed, Nat. Commun. 11 (2020) 2327;
(d) X. Shi, Z. Wu, X. Bao, Electron Energy Rev. 3 (2020) 581–612;

Please cite this article in press as: X. Gao et al., Materials Today, (2022), https://doi.org/10.1016/j.mattod.2022.07.016

(e) W. Gao, M. Pumera, Adv. Funct. Mater. 31 (2021) 2007285;
(f) S.N. Sanders et al., Nature 604 (2022) 474–478.
[5] (a) P. Chang et al., J. Mater. Chem. A 7 (2019) 4230–4258;
(b) M.P. Browne, E. Redondo, M. Pumera, Chem. Rev. 120 (2020) 2783–2810;
(c) A. Das et al., Addit. Manuf. 34 (2020) 101218;
(d) B. Bhushan, M. Caspers, Microsyst. Tehcnol. 23 (2017) 1117–1124;
(e) Y. Wang et al., Mater. 13 (2020) 466.
[6] (a) V. Egorov et al., Adv. Mater. 32 (2020) 2000556;
(b) Y. Yang et al., Appl. Energy 257 (2020) 114002;
(c) X. Tian, K. Zhou, Nanoscale 12 (2020) 7416–7432.
[7] (a) A. Miura et al., Nat. Rev. Chem. 3 (2019) 189–198;
(b) Y. Chu et al., Electro. Energy Rev. 3 (2020) 187–219;
(c) M. Weiss et al., Electro. Energy Rev. 3 (2020) 221–228;
(d) T. Chu, S. Park, K. Fu, Carbon Energy 3 (2021) 424–439.
[8] (a) S. Randau et al., Nat. Energy 5 (2020) 259–270;
(b) M. Cheng, Y. Jiang, J. Mater. Res. 22 (2021) 4547–4564;
(c) J. Ma et al., Electro. Energy Rev. 4 (2021) 545–565.
[9] (a) K. Takada, Langmuir 29 (2013) 7538–7541;
(b) Y. Xiao et al., Nat. Rev. Mater. 5 (2020) 105–126;
(c) J. Wu et al., Electro. Energy Rev. 4 (2021) 101–135;
(d) Q. Zhou et al., Adv. Mater. 31 (2019) 1902029;
(e) Z. Lv et al., Energy Storage Mater. 37 (2021) 215–223;
(f) M. Jiang et al., J. Energy Chem. 58 (2021) 300–317.
[10] K. Sun et al., *Adv. Mater.* 25 (2013) 4539–4543.
[11] K. Fu et al., *Adv. Mater.* 28 (2016) 2587–2594.
[12] (a) A.J. Blake et al., Adv. Energy Mater. 7 (2017) 1602920;
(b) D.W. McOwen et al., Adv. Mater. 30 (2018) e1707132;
(c) S.-H. Kim et al., Energy Environ. Sci. 11 (2018) 321–330.
[13] (a) S.H. Kim et al., Adv. Energy Mater. 9 (2019) 1901841;
(b) X. Gao et al., Adv. Funct. Mater. 30 (2020) 2005357;
(c) S. Anelli et al., Addit. Manuf. 51 (2022) 102636.
[14] (a) G. Kollamaram et al., Int. J. Pharm. 545 (2018) 144–152;
(b) A. Maurel et al., Sci. Repo. 9 (2019) 1–14;
(c) A. Maurel et al., Chem. Mater. 30 (2018) 7484–7493.
[15] A. Maurel et al., *J. Electrochem. Soc.* 167 (2020) 070536.
[16] S. Aston, J. Provost, H. Masselink, *J. Soc. Dye. Colour.* 109 (1993) 147–152.
[17] X. Xu et al., *Add. Manuf.* 33 (2020) 101071.
[18] S.N. Economidou et al., *Mater. Sci. Eng. C.* 102 (2019) 743–755.
[19] (a) S.H. Kim et al., Nano Lett. 15 (2015) 5168–5177;
(b) H.-D. Um et al., Energy Environ. Sci. 10 (2017) 931–940;
(c) Y. He et al., Nano Lett. 20 (2020) 7136–7143.
[20] Z. Zeng et al., Polymers 11 (2019) 956.
[21] (a) S. Huan et al., Adv. Funct. Mater. 29 (2019) 1902990;
(b) V.G. Rocha et al., J. Mater. Chem. A 8 (2020) 15646–15657.
[22] (a) P. Jiang et al., Prog. Addit. Manuf. 3 (2018) 65–86;
(b) M. Wei et al., J. Power Sources 354 (2017) 134–147;
(c) B. Guo et al., Energy Storage Mater. 39 (2021) 146–165;
(d) Y. Guo et al., Electro. Energy Rev. 4 (2021) 67–100.
[23] M. Cheng et al., *Adv. Mater.* 30 (2018) 1800615.
[24] H. Kadry et al., *Eur. J. Pharm. Sci.* 135 (2019) 60–67.
[25] M. Rosenthal et al., *Eur. J. Wood Wood* 76 (2018) 797–799.
[26] B. Cox et al., *3D Print Addit. Manuf.* 4 (2017) 116–119.
[27] (a) L. Xu et al., Joule 2 (2018) 1991–2015;
(b) C. Liu et al., Ceram. Int. 45 (2019) 14188–14197;
(c) C. Zhang et al., J. Mater. Chem. A 6 (2018) 19960–19966;
(d) S. Praveen et al., Appl. Mater. Today 26 (2022) 100980;
(e) A. Maurel et al., Addit. Manuf. 37 (2021) 101651.
[28] R.R. Kohlmeyer et al., *J. Mater. Chem.* 4 (2016) 16856–16864.
[29] J. Hu et al., *Adv. Energy Mater.* 6 (2016) 1600856.
[30] K. Shen et al., *Adv. Energy Mater.* 8 (2018) 1701527.
[31] X. Gao et al., Nano Energy 56 (2019) 595–603.
[32] (a) P. Xiao et al., Adv. Mater. 29 (2017) 1703324;
(b) Z. Gao et al., Electrochim. Acta 246 (2017) 507–516;
(c) S. Niu et al., Nano Energy 30 (2016) 138–145;
(d) Q. Pang et al., Joule 3 (2019) 136–148;
(e) X. Liang, L.F. Nazar, ACS Nano 10 (2016) 4192–4198.
[33] X. Gao et al., Energy Storage Mater. 24 (2020) 682–688.
[34] Y. Qiao et al., *Adv. Funct. Mater.* 28 (2018) 1805899.
[35] S.D. Lacey et al., *Adv. Mater.* 30 (2018) e1705651.
[36] Z. Lyu et al., *Adv. Funct. Mater.* 29 (2019) 1806658.
[37] X. Lin et al., *Chem. Mater.* 32 (2020) 3018–3027.
[38] C. Liu et al., Electrochim. Acta 314 (2019) 81–88.
[39] M.S. Saleh et al., *Addit. Manuf.* 23 (2018) 70–78.
[40] (a) J.-Y. Hwang et al., Energy Environ. Sci. 12 (2019) 2174–2184;
(b) L. Chen et al., Joule 3 (2019) 732–744;
(c) S. Zhou et al., Energy Storage Mater. 38 (2021) 141–156.
[41] K. Shen, B. Li, S. Yang, Energy Storage Mater. 24 (2020) 670–675.
[42] X. Gao et al., *Adv. Energy Mater.* 10 (2020) 1903753.
[43] D. Lee et al., *Adv. Mater.* 32 (2020) 1905573.
[44] (a) H.D. Asfaw et al., Energy Tech. 7 (2019) 1900797;
(b) K. Miyamoto et al., Isci. 23 (2020) 101317;
(c) J. Ni, L. Li, Adv. Funct. Mater. 28 (2018) 1704880;
(d) B. Sun et al., ACS Appl. Mater. Interfaces 10 (2018) 2407–2413;
(e) C. Yue, J. Li, L. Lin, Front. Mech. Eng. 12 (2017) 459–476;
(f) J.S. Park, T. Kim, W.S. Kim, Sci. Rep. 7 (2017) 3246.
[45] H. Ragones et al., Sustain. Energy Fuels 2 (2018) 1542–1549.
[46] C. Reyes et al., Energy Mater. 1 (2018) 5268–5279.
[47] L. Zhou et al., Adv. Mater. Technol. (2018) 1800402.
[48] (a) T.S. Wei et al., Adv. Mater. 30 (2018) 1703027;
(b) Y. Bao et al., Energy Stor. Mater. 33 (2020) 55–61.
[49] (a) Z. Lin, X. Guo, H. Yu, Nano Energy 41 (2017) 646–653;
(b) Y. Zhang et al., Angew. Chem. Int. Ed. Engl. 59 (2020) 7797–7802;
(c) G. Li et al., Nat. Energy 3 (2018) 1076–1083.
[50] X. Zhou et al., *J. Membr. Sci.* (2020) 117820.
[51] T. Ates et al., Energy Storage Mater. 17 (2019) 204–210.
[52] Y. Ji et al., Mater. 13 (2020) 560.
[53] (a) X. Yang et al., Energy Storage Mater. 27 (2020) 198–204;
(b) X. Yang et al., Energy Environ. Sci. 13 (2020) 1318–1325.
[54] (a) X. Li et al., Energy Environ. Sci. 12 (2019) 2665–2671;
(b) X. Li et al., Angew. Chem. 131 (2019) 16579–16584;
(c) X. Li et al., Nano Lett. 20 (2020) 4384–4392.
[55] (a) D. Lei et al., Nat. Commun. 10 (2019) 1–11;
(b) M. Zhu et al., J. Energy Chem. 37 (2019) 126–142;
(c) X. Wang et al., Compos. B Eng. 110 (2017) 442–458.
[56] (a) M. Suleman et al., J. Alloy. Compd. 695 (2017) 3376–3392;
(b) Y. Liu et al., Adv. Funct. Mater. 28 (2018) 1706592.
[57] (a) Z. Xie et al., J. Membr. Sci. 586 (2019) 122–129;
(b) J. Rao et al., Nano Energy 51 (2018) 425–433;
(c) Q. Pang et al., Nat. Energy 3 (2018) 783–791.
[58] P.E. Delannoy et al., *J. Power Sources* 274 (2015) 1085–1090.
[59] Y. Wang et al., *Adv. Funct. Mater.* 27 (2017) 1703140.
[60] L.J. Deiner et al., *Adv. Eng. Mater.* 21 (2019) 1900952.
[61] Z. Zhao, H. Wu, Nano Res. 12 (2019) 2477–2484.
[62] H. Ragones et al., J. Electrochem. Soc. 167 (2020) 070503.
[63] X. Yang et al., *Adv. Mater.* 31 (2019) 1901220.
[64] (a) X. Gao et al., Adv. Funct. Mater. 29 (2019) 1806724;
(b) X. Yang et al., J. Mater. Chem. A 6 (2018) 22958–22965.
[65] (a) X. Huang et al., J. Power Sources 382 (2018) 190–197;
(b) Y. Lu et al., Energy Storage Mater. 15 (2018) 282–290.
[66] X. Yang, J. Luo, X. Sun, *Chem. Soc. Rev.* 49 (2020) 2140–2195.
[67] X. Yang et al., *Electrochem. Energy Rev.* 1 (2018) 239–293.
[68] (a) X. Li et al., Energy Environ. Sci. 11 (2018) 2828–2832;
(b) X. Li et al., Adv. Mater. 31 (2019) 1808100;
(c) K. Iwase et al., ACS Appl. Energy Mater. 4 (2021) 3651–3659.
[69] (a) X. Gao et al., J. Mater. Chem. A 8 (2020) 278–286;
(b) C. Shen et al., Electrochim. Acta 349 (2020) 136331.
[70] (a) H. Huo et al., Energy Storage Mater. 29 (2020) 361–366;
(b) H. Huo et al., Nano Energy (2020) 104836;
(c) M. Mahmoudi et al., ACS Appl. Mater. Interfaces 12 (2020) 31984–31991.
[71] H. Xie et al., ACS Energy Lett. 4 (2019) 2668–2674.
[72] S. Zekoll et al., Energy Environ. Sci. 11 (2018) 185–201.
[73] D. Cao et al., *Adv. Mater.* 31 (2019) e1807313.
[74] W.J. Sames et al., Int. Mater. Rev. 61 (2016) 315–360.
[75] (a) A. Vafadar et al., Appl. Sci. 3 (2021) 11;
(b) A. Gisario et al., J. Manuf. Syst. 53 (2019) 124–149.
[76] E.O. Olakanmi, R.F. Cochrane, K.W. Dalgarno, Prog. Mater Sci. 74 (2015) 401–477.
[77] C.Y. Yap et al., Appl. Phys. Rev. 2 (2015) 041101.
[78] C. Körner, International Mater. Rev. 61 (2016) 361–377.
[79] (a) M. Javidani et al., J. Therm. Spray Technol. 26 (2017) 587–597;
(b) A. Maurel et al., IEEE Access 9 (2021) 140654–140666.
[80] M. Ziaee, N.B. Crane, *Addit. Manuf.* 28 (2019) 781–801.
[81] K.A. Ibrahim, B. Wu, N.P. Brandon, *Mater. Design* 106 (2016) 51–59.
[82] A. Maurel et al., *Addit. Manuf.* 37 (2021) 101651.
[83] K.A. Acord et al., *J. Mater. Sci.* 288 (2021) 116827.

Please cite this article in press as: X. Gao et al., Materials Today, (2022), https://doi.org/10.1016/j.mattod.2022.07.016

[84] (a) M.S. Onses et al., Small 11 (2015) 4237–4266;
(b) A. Azhari et al., Carbon 119 (2017) 257–266.
[85] B.W. An et al., *Adv. Mater.* 27 (2015) 4322–4328.
[86] Y. Wu, J. Y. H. Fuh, Y. S. Wong, J. Sun, presented in part at the ASME 2015 *International Manufacturing Science and Engineering Conference*, **2015**.
[87] Y. Yang et al., Biomater. 230 (2020) 119618.
[88] J.-U. Park et al., Nano Lett. 8 (2008) 4210–4216.
[89] A. Reiser et al., *Nat. Commun.* 10 (2019) 1853.
[90] H. Lee et al., Small 10 (2014) 3918–3922.
[91] (a) Y. Yang et al., Adv. Mater. 29 (2017) 1605750;
(b) Y. Yang et al., Sci. Adv. 5 (2019) 9490.
[92] G.L. Goh, S. Agarwala, W.Y. Yeong, *Adv. Mater. Interfaces* 6 (2019) 1801318.
[93] J. Shaver et al., ACS Nano 3 (2009) 131–138.
[94] J. Hone et al., *Appl. Phys. Lett.* 77 (2000) 666–668.
[95] M. Liu et al., Polymer 166 (2019) 81–87.
[96] D. Kokkinis, M. Schaffner, A.R. Studart, *Nat. Commun.* 6 (2015) 8643.
[97] X. Zhou, Y. Hou, J. Lin, AIP Adv. 5 (2015) 030701.
[98] E. Pei, Assembly Autom. 34 (2014) 123–127.
[99] F. Momeni et al., *Mater. Design* 122 (2017) 42–79.
[100] (a) J. Mohd Jani et al., Mater. Design 56 (2014) 1078–1113;
(b) Q. Ge et al., Sci. Rep. 6 (2016) 31110;
(c) Z. Zhang, K.G. Demir, G.X. Gu, Int. J. Smart Nano Mater. 10 (2019) 205–224.
[101] (a) A. Sydney Gladman et al., Nat. Mater. 15 (2016) 413–418;
(b) S. Joshi et al., Appl. Mater. Today 18 (2020) 100490.
[102] (a) F. Momeni et al., Mater. Design 122 (2017) 42–79;
(b) A.S. Gladman et al., Nat. Mater. 15 (2016) 413–418.
[103] M.C. Mulakkal et al., *Mater. Design* 160 (2018) 108–118.
[104] (a) Z. Zhang, K.G. Demir, G.X. Gu, Int. J. Smart Nano Mater. 10 (2019) 20;
(b) H.A. Alshahrani, J. Sci. Adv. Mater. Dev. 6 (2021) 167–185.
[105] R. Ammoun et al., *J. Prosthodont.* 30 (2021) 71–75.
[106] J.-X.-Y. Lim, Q.-C. Pham, Virtual. Phys. Prototyp. 16 (2021) 333–346.
[107] A. du Plessis, E. Macdonald, *Addit. Manuf.* 34 (2020) 101191.
[108] S. Ji, M. Guvendiren, Front. Bioeng. Biotechnol. 5 (2017) 23.
[109] S. Tagliaferri, A. Panagiotopoulos, C. Mattevi, *Mater. Adv.* 2 (2021) 540–563.
[110] J. Nsengimana et al., Rapid Prototype J. 25 (2019) 1–12.
[111] M.R. Khosravani et al., Polymers 10 (2021) 13.
[112] M. Mu et al., Addit. Manuf. 31 (2020) 100972.

Please cite this article in press as: X. Gao et al., Materials Today, (2022), https://doi.org/10.1016/j.mattod.2022.07.016